

Trace gas evolution in the lowermost stratosphere from Aura Microwave Limb Sounder measurements

M. L. Santee,¹ G. L. Manney,^{1,2} N. J. Livesey,¹ L. Froidevaux,¹ M. J. Schwartz,¹ and W. G. Read¹

Received 6 January 2011; revised 17 June 2011; accepted 28 June 2011; published 24 September 2011.

[1] Daily global measurements from NASA's Aura Microwave Limb Sounder (MLS) allow comprehensive investigation of interhemispheric and interannual variations in chemical and transport processes throughout the lowermost stratosphere (LMS). We analyze nearly seven years of MLS O₃, HNO₃, HCl and ClO measurements along with meteorological analyses to place chemical processing in and dispersal of processed air from the winter polar lowermost vortex and subvortex in a global context. The MLS data, the first simultaneous observations of HCl and ClO covering much of the LMS, reveal that chlorine activation is widespread in the Antarctic subvortex and can occur to a significant degree in the Arctic subvortex. Unusually low temperatures and strong, prolonged chlorine activation in the lowermost vortex and subvortex promoted large ozone losses there in the 2006 (and 2008) Antarctic and 2004/2005 Arctic winters, consistent with reported record low column ozone. Processed air dispersing from the decaying vortex in spring induces rapid changes in extravortex trace gas abundances. After vortex breakdown, the subtropical jet/tropopause becomes the major transport barrier in the LMS. Quasi-isentropic transport of tropical tropospheric air into the LMS, associated with the summer monsoon circulations, leads to decreases in extratropical O₃, HNO₃, and HCl in both hemispheres. Strong mixing in the summertime LMS homogenizes extratropical trace gas fields. MLS measurements in the tropics show signatures of monsoon-related cross-equatorial stratosphere-to-troposphere transport. Observed seasonal and interannual variations in trace gas abundances in the LMS are consistent with variations in the strength of transport barriers diagnosed from meteorological analyses.

Citation: Santee, M. L., G. L. Manney, N. J. Livesey, L. Froidevaux, M. J. Schwartz, and W. G. Read (2011), Trace gas evolution in the lowermost stratosphere from Aura Microwave Limb Sounder measurements, *J. Geophys. Res.*, 116, D18306, doi:10.1029/2011JD015590.

1. Introduction

[2] Although chemical processing in the lower stratospheric winter polar vortices has been the subject of intense scrutiny for more than two decades, less attention has been focused specifically on the lowermost stratosphere (LMS), a distinct region traditionally defined to lie between the local tropopause and the isentrope corresponding to the tropical tropopause (typically 380 K) [e.g., Holton *et al.*, 1995; Shepherd, 2007]. The mass of the LMS fluctuates as the heights of the tropopause and the 380 K surface vary with season [e.g., Appenzeller *et al.*, 1996; Schoeberl, 2004]. Air enters the LMS mainly through diabatic downwelling from the stratosphere or adiabatic quasi-horizontal transport and mixing from the tropical and subtropical upper tropo-

sphere. Episodic diabatic upward transport from the extratropical troposphere occurs via deep (or sporadic pyro) convection [e.g., Poulard *et al.*, 1996; Fu *et al.*, 2006; Fromm *et al.*, 2010] and synoptic-scale frontal uplift [e.g., Rood *et al.*, 1997; Stohl *et al.*, 2003]. Other small-scale transient processes, such as tropopause folds and cutoff lows, can also promote the exchange of air between the LMS and the troposphere in the extratropics [e.g., Stohl *et al.*, 2003; Shepherd, 2007]. As a consequence of all of these mechanisms, air in the extratropical LMS bears both stratospheric and tropospheric characteristics [e.g., Lelieveld *et al.*, 1997; Hintsa *et al.*, 1998; Ray *et al.*, 1999; Pan *et al.*, 2004; Hoor *et al.*, 2005; Hegglin *et al.*, 2006, 2009; Pittman *et al.*, 2007; Bönisch *et al.*, 2009].

[3] In addition to large- and small-scale dynamical processes, the composition of the LMS is affected by local chemical and microphysical processes. For example, polar stratospheric clouds (PSCs) sequester gas-phase HNO₃ and H₂O and provide surfaces on which heterogeneous reactions convert chlorine from reservoir to reactive forms. Although PSCs are only rarely observed below ~15 km in the Arctic [e.g., Massoli *et al.*, 2006; Fromm *et al.*, 1999; Pitts *et al.*,

¹Jet Propulsion Laboratory, California Institute of Technology, Pasadena, California, USA.

²Also at Department of Physics, New Mexico Institute of Mining and Technology, Socorro, New Mexico, USA.

2009], they are present at these altitudes during much of the winter in the Antarctic [e.g., *Fromm et al.*, 1997; *Adriani et al.*, 2004; *Pitts et al.*, 2009]. Moreover, the signature of HNO₃ vertical redistribution into the LMS through sedimentation and subsequent evaporation of PSCs from above (renitrification) has been identified in both the Arctic [e.g., *Hübner et al.*, 1990; *Fischer et al.*, 1997; *Arnold et al.*, 1998; *Kondo et al.*, 2000; *Irie et al.*, 2001; *Koike et al.*, 2002; *Dibb et al.*, 2006] and Antarctic [*Hofmann and Deshler*, 1991]. Although appreciable abundances of reactive chlorine (of up to a few tens of pptv) in the Northern Hemisphere middle- and high-latitude lower/uppermost stratosphere have been linked to activation on background or volcanically enhanced sulfate aerosols or cirrus ice clouds [*Avallone et al.*, 1993; *Keim et al.*, 1996; *Borrmann et al.*, 1996, 1997; *Thornton et al.*, 2003, 2007], substantial enhancements in ClO (of several tenths of a ppbv or more), comparable to those routinely measured at higher altitudes arising from PSC activity, have not been reported below 380 K in the Arctic. Nevertheless, significant chemical ozone loss has been diagnosed in the lowermost vortex in a few Arctic winters [e.g., *Bregman et al.*, 1997; *Knudsen et al.*, 1998; *Rex et al.*, 2006; *Tilmes et al.*, 2008]. In contrast, considerably elevated levels of reactive chlorine in the LMS have been recorded in the southern polar regions [*Anderson et al.*, 1989; *Brune et al.*, 1989]. Furthermore, calculations along aircraft flight tracks have shown that maximum ozone loss rates over Antarctica can actually occur below 400 K [*Murphy*, 1991]. More recently, using a three-dimensional chemical transport model and ozonesonde observations, *Lee et al.* [2002] found substantial in situ ozone destruction in the Antarctic LMS. Indeed, *Lee et al.* [2002] estimated that more than a quarter of the ozone loss associated with the Antarctic ozone hole occurs in the LMS, with the contribution to the decline in ozone at these levels from the descent of O₃-poor air from the vortex aloft only becoming significant after mid-October.

[4] The export of chemically processed and ozone-depleted air from the polar vortex in late winter and early spring can significantly affect extratropical trace gas distributions [e.g., *World Meteorological Organization*, 2007a]. Chemically perturbed air is largely confined within the polar vortex until its breakdown at the end of the winter, but the degree of containment varies substantially with altitude. *McIntyre* [1995] termed the region below the strong confinement of the vortex proper the “subvortex”. He noted that, like the vortex itself, the subvortex is a region of low temperatures and chemical processing, but tropospheric weather activity prevents the formation of a well-defined “edge” (i.e., transport barrier), and much more vigorous stirring efficiently transports air between polar and middle latitudes. Previously, aircraft observations obtained during the Airborne Antarctic Ozone Experiment (AAOE) had revealed a marked change in the dynamical character of the polar vortex near 400 K potential temperature, with the different chemical signature of trace species below this level consistent with greater exchange between polar and midlatitude air [e.g., *Tuck*, 1989]. Numerical studies of the isolation of the polar vortex had also suggested the presence of a transition layer near 400 K, above which the edge of the vortex constitutes a very strong barrier to mass exchange and below which the permeability of the vortex edge increases substantially [e.g., *Bowman*, 1993; *Chen*, 1994; *Chen et al.*, 1994]. In line with

these results, *McIntyre* [1995] placed the vortex/subvortex transition altitude at about 400 K.

[5] *Manney et al.* [1994] showed, however, that the degree of mixing between polar and midlatitude air depends strongly on the position and evolution of the polar night jet (which moves downward as winter progresses) and on the amount of descent experienced by air parcels; consequently, it exhibits considerable interannual variability in both hemispheres. Using a diagnostic of the degree of mixing, *Haynes and Shuckburgh* [2000a, 2000b] found that the 400-K isentrope has no particular significance in either hemisphere; rather, the vortex/subvortex transition is gradual and varies substantially in altitude over the winter/spring period, from about 350 to 380 K in the Southern Hemisphere and from about 400 to above 450 K in the Northern Hemisphere. Similar seasonal variations in the depth of the winter polar vortex transport barriers were also found by *Allen and Nakamura* [2001].

[6] As climate change affects the upper troposphere/lower stratosphere (UTLS) region in the coming decades, subvortex chemical processing may have important implications for recovery of the Antarctic ozone hole, as well as for the possibility of more severe ozone depletion in the Arctic. Changes in the chemical composition of the UTLS, in particular ozone, may in turn strongly affect atmospheric radiative forcing [e.g., *Lacis et al.*, 1990; *Forster and Shine*, 1997]. Moreover, as mentioned earlier, the efficient exchange between polar and lower-latitude air at these levels spreads the influence of polar processing throughout the extratropics. Therefore, to improve our prognostic capability it is essential to obtain a better understanding of the distribution and variability of trace gases in the UTLS, as well as the underlying chemical and dynamical processes that control them. Daily global measurements from the Microwave Limb Sounder (MLS) on NASA’s Aura satellite, launched in July 2004, have enabled the first comprehensive multiyear examination of chemical processing and transport in the LMS and subvortex in both hemispheres. Here we analyze nearly seven years of MLS O₃, HNO₃, HCl, and ClO observations to investigate the interhemispheric and interannual variations in chemical processing and in the evolution of transport barriers in the LMS and subvortex regions.

2. Measurement Description

[7] MLS measures millimeter- and submillimeter-wavelength thermal emission from the limb of Earth’s atmosphere [*Waters et al.*, 2006]. The Aura MLS fields of view point in the direction of orbital motion and vertically scan the limb in the orbit plane, leading to data coverage from 82°S to 82°N latitude on every orbit. Because the Aura orbit is sun-synchronous (with a 1345 local time ascending equator-crossing time), MLS observations at given latitudes on either the ascending (mainly day) or descending (mainly night) portions of the orbit have approximately the same local solar time. Northern high latitudes are sampled by ascending measurements near midday local time, whereas southern high latitudes are sampled by ascending measurements in the late afternoon.

[8] This study uses version 3.30 (v3.3) MLS measurements of O₃, HNO₃, HCl, and ClO in the UTLS. Detailed information on the quality of the previous version of MLS data, v2.2, can be found in validation papers by *Livesey et al.*

Table 1. Summary of Aura MLS v3.3 Measurement Characteristics in the UTLS

MLS Product	Resolution Vertical \times Horizontal ^a (km)	Precision ^b
O ₃	2.5–3 \times 300–450	± 0.03 to ± 0.1 ppmv
HNO ₃	3–4 \times 350–500	± 0.7 to ± 1.2 ppbv
HCl	3 \times 200–400	± 0.2 to ± 0.4 ppbv
CIO	3–4.5 \times 300–600	± 0.1 to ± 0.3 ppbv

^aHorizontal resolution in along-track direction; cross-track resolution is 10 km or less for all species, and the separation between adjacent retrieved profiles along the measurement track is 1.5° great circle angle (~165 km).

^bPrecision on individual profiles. For most of these species, the larger (i.e., poorer) precision (and resolution) values apply to the lowest retrieval levels.

[2008a] and *Froidevaux et al.* [2008a] for upper tropospheric and stratospheric ozone, respectively, *Santee et al.* [2007] for HNO₃, *Froidevaux et al.* [2008b] for HCl, and *Santee et al.* [2008a] for CIO. The recently released v3.3 MLS data processing algorithms have led to notable improvements in several products, in particular HNO₃ and CIO (discussed below).

[9] The precision, resolution, and useful vertical range of the v3.3 measurements, as well as some preliminary assessments of their accuracy through initial validation comparisons with correlative data sets, are reported for each species in the v3.3 Level 2 data quality and description document [*Livesey et al.*, 2011]. Table 1 briefly summarizes the precision and resolution of the relevant v3.3 data in the UTLS. Note that the range of reliable measurements extends down to the 261-hPa MLS retrieval pressure surface for O₃, the 215-hPa level for HNO₃, and the 147-hPa level for HCl and CIO. The single-profile precision estimates given here can be improved by averaging; for the averaged quantities on which most of the conclusions of this study are based, the estimated precisions are smaller by about a factor of 10 than the values in Table 1.

[10] The vertical resolution of MLS profiles can be quantified as the full width at half maximum of the “averaging kernels” (*Livesey et al.* [2006, 2011]; see also the respective validation papers for individual products). The MLS averaging kernels are “sharp” functions (not, for example, boxcar averages), and their relative sharpness enables realistic depiction of atmospheric structure on length scales somewhat finer than the averaging kernel widths. Although MLS measurements have previously been shown to accurately characterize the large-scale morphology of several trace gases in the UTLS [e.g., *Livesey et al.*, 2008b; *Santee et al.*, 2007], their ability to discriminate features of small vertical scale is just beginning to be explored in detail. *Manney et al.* [2009b, 2011] demonstrated that, despite their nominal vertical resolution in the UTLS (2.5–4.5 km, depending on the species), MLS data successfully capture distinct, relatively localized vertical structure in trace gas distributions in this region. The results presented in the following sections confirm that, as expected based on measurement simulations (not shown), realistic aspects of atmospheric structure on height scales shorter than those quoted in Table 1 are accurately represented in MLS data.

[11] Ozone in the UTLS is retrieved on twice as fine a vertical grid in v3.3, leading to better vertical resolution than in v2.2. Biases in O₃ in the upper troposphere have also been

reduced [*Livesey et al.*, 2011]. Comparisons with various ground-based, balloon-borne, and satellite data sets indicated that the MLS v2.2 HNO₃ values are biased low by 10–30% throughout most of the vertical range, and possibly more at 215 hPa [*Santee et al.*, 2007]. This low bias has been largely eliminated in v3.3 HNO₃ data, which generally show much closer agreement with correlative data sets [*Livesey et al.*, 2011]. In general, the v3.3 HCl retrievals have changed little from those in v2.2 [*Livesey et al.*, 2011]. Mixing ratios have increased slightly at 100 hPa and also at 147 hPa, at which level a high bias in HCl has worsened, particularly in the tropics, where data below 100 hPa are not recommended for scientific use. HCl measurements at 147 hPa may be used outside of the tropics, however. As discussed in detail by *Santee et al.* [2008a], a considerable latitudinally varying negative bias is present in the v2.2 CIO values at retrieval pressures larger than 22 hPa. In v3.3, the bias in the CIO data has been essentially eliminated at retrieval pressures less than 68 hPa and substantially mitigated elsewhere. Moreover, the remaining small biases at 68, 100, and 147 hPa (the latter not formerly a recommended level) have been better characterized, and a pressure- and latitude-dependent bias correction [*Livesey et al.*, 2011] is applied to the v3.3 CIO data shown here before they are vertically interpolated to potential temperature surfaces.

[12] One respect in which the quality of the MLS UTLS data has not been improved in v3.3 is their sensitivity to clouds, as retrievals at the lowest levels are more adversely affected by the presence of thick clouds (i.e., ice particles in convective cores) than they were in v2.2. Such cloud effects can lead to unphysical values, particularly in the equatorial region. Detailed instructions for screening to remove tropical cloud-induced outliers (along with other poor-quality data points) in the HNO₃ and O₃ products are given in the v3.3 data quality document [*Livesey et al.*, 2011] and are followed here. Attempts to filter cloud-affected data points in the tropical UTLS have so far been less successful for v3.3 HCl and CIO. More efficacious cloud-screening procedures are currently under development, but the results shown here, especially for CIO, still include some unrealistic values in the tropical UTLS attributable, at least in part, to cloud artifacts.

[13] In addition to MLS measurements, this study makes extensive use of meteorological data from the NASA Global Modeling and Assimilation Office (GMAO) Goddard Earth Observing System Versions 5.1.0 and 5.2.0 analyses, either from the operational near-real-time (NRT) system [*Reinecker et al.*, 2008] or from the Modern Era Retrospective-analysis for Research and Applications (MERRA) 32-year reanalysis [*Bosilovich et al.*, 2008; *Reinecker et al.*, 2011] (both referred to hereinafter as GEOS-5). The GEOS-5 analysis is performed by the Gridpoint Statistical Interpolation (GSI) [*Wu et al.*, 2002]; the analysis correction pulling the forecast model toward the observations is then applied gradually through incremental analysis updates (IAU) [*Bloom et al.*, 1996]. GEOS-5 analyses are provided on a 1/2° latitude by 2/3° longitude grid, on 72 terrain-following model levels from the surface through the stratosphere, and with analyses every six hours. Along with standard meteorological variables, GEOS-5 products include an expansive set of fields from the model and assimilation system, including diabatic heating rates and potential vorticity (PV) calculated internally in the model. For most of the work presented here, we use

the MERRA reanalyses. However, unlike the other fields, MERRA PV is produced on pressure levels on a reduced-resolution grid, rather than on model levels on the full-resolution grid. Therefore, the NRT analyses are used for all PV overlays on figures. On the other hand, MERRA PV is used in the calculation of effective diffusivity (discussed further in section 4), for which a smoother PV field on a coarser grid is advantageous. Throughout this paper, absolute values are used whenever PV is specified.

3. Seasonal and Interannual Variations in the Lowermost Vortex and Subvortex

[14] As an illustration of chemical and dynamical variability in the lowermost vortex and subvortex, we begin with maps of MLS data for a representative day during the 2006 Antarctic late winter (Figure 1). The data have been interpolated to several potential temperature surfaces in the UTLS; note, however, that because of the vertical resolution of the measurements (see Table 1), the values obtained at these levels are not completely independent. The 410 and 390 K surfaces reside within the lower stratosphere, whereas the 370 and 350 K surfaces represent the upper portion of the LMS in the extratropics. On all maps, black overlays (showing the 1.2 and $1.4 \times 10^{-4} \text{ s}^{-1}$ contours of scaled PV, sPV) demarcate the approximate boundary of the polar vortex. White overlays identify the approximate location of the dynamical (PV) tropopause. As discussed by Stohl *et al.* [2003], the exact definition of the dynamical tropopause remains somewhat subjective, and a wide range of PV values has been employed [e.g., Pan *et al.*, 2004, 2007; Krebsbach *et al.*, 2006; Schoeberl, 2004; Scott *et al.*, 2003; Highwood *et al.*, 2000; Haynes and Shuckburgh, 2000b, and references therein]. Recently, Kunz *et al.* [2011] identified the location of the extratropical dynamical tropopause on isentropic surfaces by the maximum in the PV gradient with respect to equivalent latitude; the PV value associated with this gradient-based tropopause generally increases with increasing potential temperature, especially in the Southern Hemisphere, and, depending on the season, ranges between 1.5 and 5.0 PVU (where $1 \text{ PVU} = 10^{-6} \text{ Km}^2 \text{ kg}^{-1} \text{ s}^{-1}$). Here we use the 4.5 PVU contour, as recommended by Haynes and Shuckburgh [2000b] for the 370-K level; Scott *et al.* [2003] found that the region of weakest mixing indicative of the tropopause corresponds to PV values of ~ 4 PVU in the Northern Hemisphere and ~ 5 PVU in the Southern Hemisphere during winter at 370 K, and Krebsbach *et al.* [2006] and Pan *et al.* [2007] also found that air masses with PVU values of 4 or greater are characterized by stratospheric ozone abundances.

[15] The high values of O_3 and HNO_3 in the so-called “collar” region along and inside of the vortex edge reflect the seasonal buildup of these species as a consequence of relatively confined diabatic descent (the descending branch of the Brewer-Dobson circulation). By late winter, O_3 and HNO_3 are both severely depleted poleward of the collar region at 410 K. Substantial (though increasingly localized) depletion in HNO_3 is evident down to 350 K, as are the effects of chemical ozone destruction, which continues to intensify at these levels into October in 2006. The contours of O_3 and HNO_3 at all levels (and of the tracer CO below 410 K, not shown) suggest an episode of mixing from the edge into the interior of the vortex near 140°E longitude, south of

Australia. Reverse domain-filling trajectory calculations (not shown) provide additional support for the occurrence of significant transport between the vortex edge and core regions, as well as for the mixing of some lower-latitude air into the vortex. A greater degree of permeability in the vortex edge in this region is also implied by the weakened PV gradients (note the increased separation between the two black contours) below 410 K. Inspection of maps for neighboring days indicates that this mixing event is fairly short-lived. Although in general the vortex is sufficiently robust in this season to inhibit large-scale exchange between polar and midlatitude air at all levels, spatially and temporally limited transport events such as this abound in the MLS data record.

3.1. Southern Hemisphere Seasonal Variations

[16] We examine the evolution of the Southern Hemisphere vortex/subvortex in more detail in Figures 2 and 3, which show snapshots of the UTLS on selected days during the 2006/2007 late winter, spring, and summer as a function of equivalent latitude (EqL) and potential temperature (θ). EqL, the latitude encircling the same area as a given contour of PV [Butchart and Remsberg, 1986], is used to provide a vortex-centered view in which meteorologically similar air masses are averaged together. As described by Manney *et al.* [1999, 2007], the cross sections are produced by taking weighted averages of MLS measurements around each grid point. In this procedure, all data points falling within prescribed envelopes in EqL and $\ln(\theta)$ of a given grid location are weighted by their distance from it. The resulting averages are fairly insensitive to the type of weighting function employed; here we use a Gaussian. The half width in EqL is 2° . Slightly different vertical grids (and half-widths) are used for different species, depending on their specific vertical resolution and the number of points in each grid box; e.g., a finer vertical grid is appropriate for ozone, commensurate with its higher vertical resolution, whereas a coarser grid is necessary for ClO, for which only daytime measurements are used. Only data within two half-widths in EqL and one half-width in $\ln(\theta)$ of the grid point are included in the average. In addition to being weighted by distance, the values averaged at each grid location are weighted by the measurement uncertainty using the same function as for the spatial weighting, with the error half-width and cutoff determined by the estimated precision for each species. Although the error weighting allows inclusion of almost all measurement points, occasional poor-precision profiles that fall far out in the wings of the Gaussian are given very little weight. In this manner the closest and most precise measurements contribute most strongly to the averages at each grid point.

[17] The 1.5 and 4.5 PVU contours overlaid in white on all panels bracket the probable region of the tropopause. The horizontal white line marks 380 K; the region below that line poleward of the tropopause is the upper portion of the LMS. The black lines are contours of normalized PV gradient, identifying the locations of the EqL-averaged representation of the transport barriers associated with the Antarctic vortex (near 60°S) and the upper tropospheric subtropical jet (near $30\text{--}40^\circ\text{S}$). The subtropical jet/tropopause barrier is seen to tilt poleward at lower altitudes, as shown also by Haynes and Shuckburgh [2000b], especially as the year progresses. Although considerable day-to-day variability occurs in these

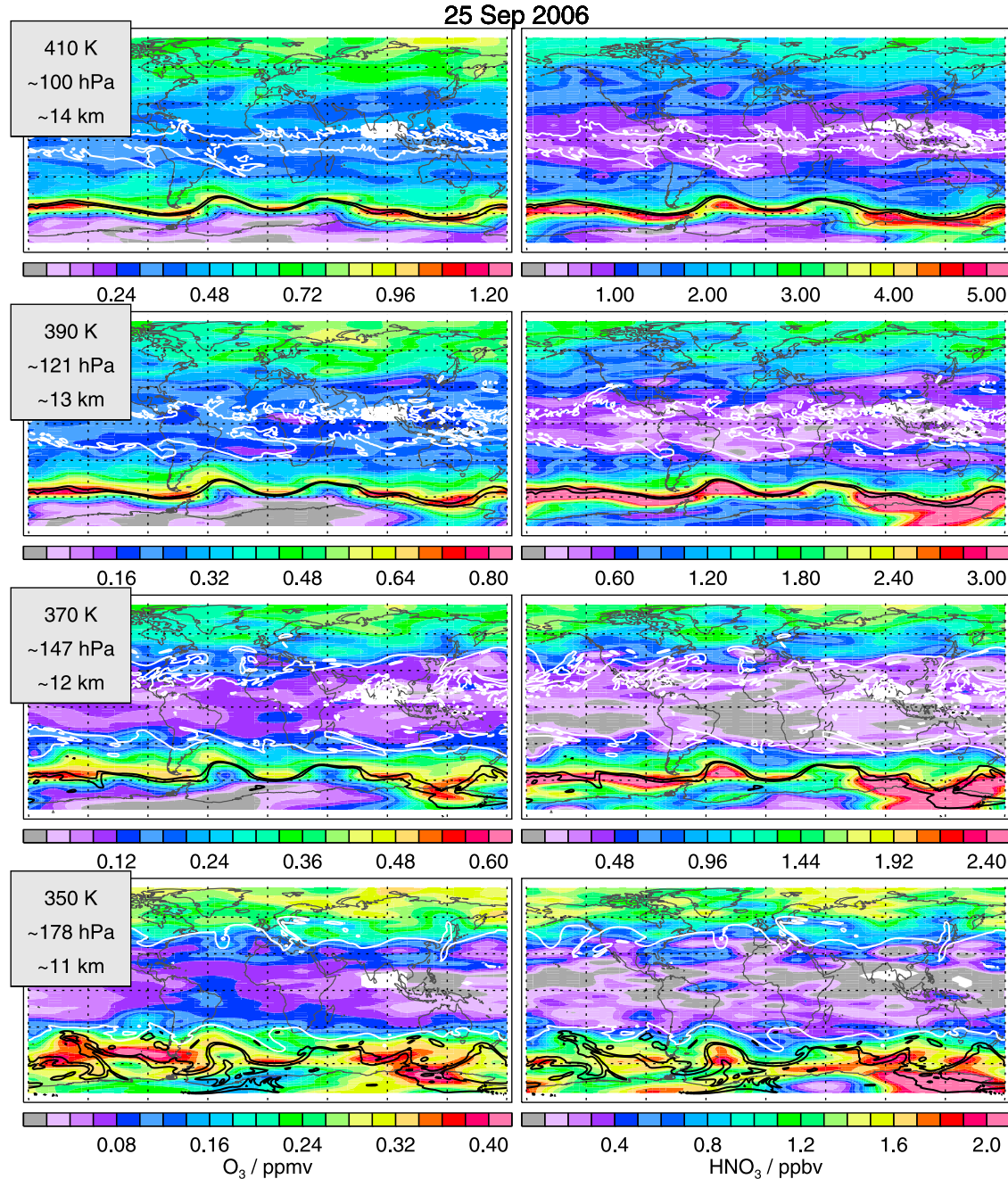


Figure 1. Maps of version 3.30 (v3.3) MLS (left) O₃ and (right) HNO₃ for a day in the 2006 Antarctic late winter, interpolated to potential temperature surfaces using Global Modeling and Assimilation Office Goddard Earth Observing System (GEOS-5) temperatures. Corresponding approximate pressures and altitudes in the extratropics are given in the legend for each potential temperature surface. White lines show the $4.5 \times 10^{-6} \text{ K m}^2 \text{ kg}^{-1} \text{ s}^{-1}$ (4.5 PVU) GEOS-5 potential vorticity (PV) contour to identify the dynamical tropopause. Solid black lines represent the 1.2 and $1.4 \times 10^{-4} \text{ s}^{-1}$ contours of scaled PV (sPV, calculated using the method of Manney *et al.* [1994]) to demarcate the polar vortex boundary; two contours are shown to give a sense of the strength of the vortex and its degree of impermeability.

fields, the dates shown in Figure 2 are representative of their respective mid-month periods.

3.1.1. August

[18] In mid-August, the polar night jet extends to just below 380 K. According to the GEOS-5 diabatic heating rates (not shown), air is descending in most of the southern middle

and high latitude lower/lowermost stratosphere at this time. Ozone abundances are high throughout the vortex/subvortex. In contrast, HNO₃ is depleted down to (and even below) the bottom of the vortex. Because MLS measures HNO₃ only in the gas phase, we cannot distinguish whether the observed depression is due to sequestration in extant PSCs, which are

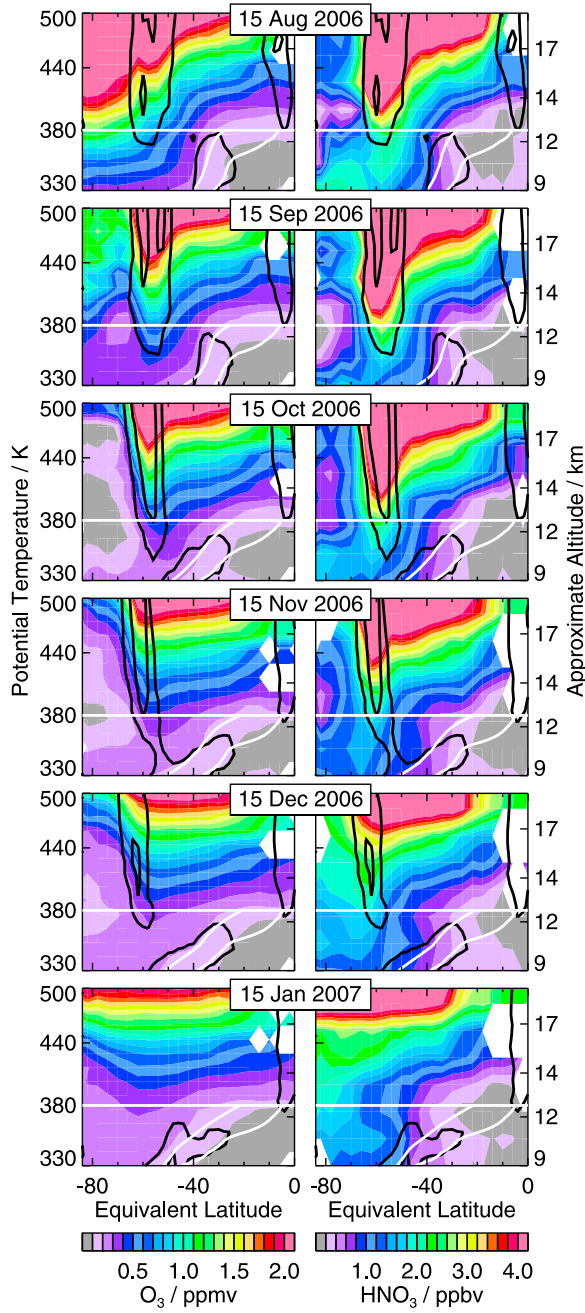


Figure 2. Equivalent latitude/potential temperature (EqL/θ) cross sections of v3.3 MLS (left) O_3 and (right) HNO_3 measurements, for six selected days during the 2006/2007 Antarctic late winter, spring, and summer. The vertical domain of the panels spans the range from roughly 130–220 hPa (330 K) to 30–50 hPa (500 K), depending on the temperature; corresponding approximate altitudes in the extratropics are given on the right-hand axis. Black contours represent GEOS-5 normalized PV gradients of 1.5 and 4.5; values greater than 1 indicate stronger-than-average gradients. White contours show 1.5 and 4.5 PVU values to delineate the tropopause; the horizontal white line marks the 380-K potential temperature surface.

typically present in the Antarctic LMS in mid-August [Hofmann and Deshler, 1991; Fromm et al., 1997; Adriani et al., 2004; Pitts et al., 2009], or irreversible denitrification, which occurs when PSC particles grow large enough to sediment at an appreciable rate. Since denitrification

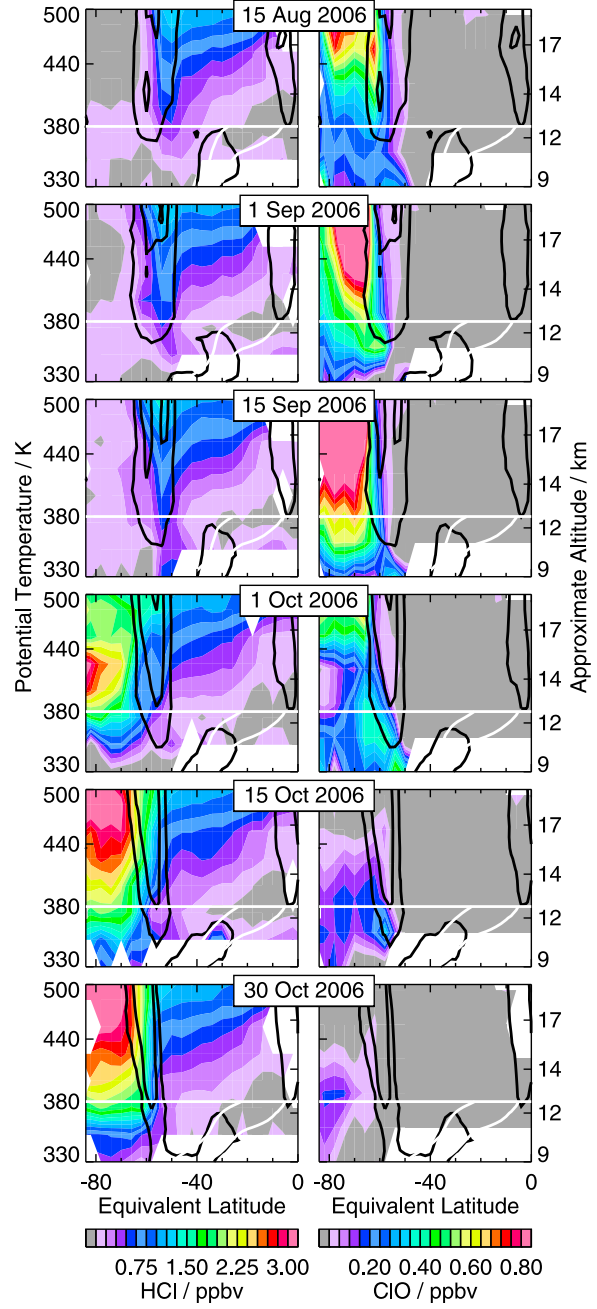


Figure 3. EqL/θ cross sections of v3.3 MLS (left) HCl and (right) CIO, for six selected days during the 2006 Antarctic late winter and spring. Different dates are shown for these species than for O_3 and HNO_3 to more closely track the progression of chlorine activation/deactivation. Only daytime measurements are used for CIO. The sharp cutoff arises because HCl and CIO are not retrieved at pressures larger than 147 hPa, and thus these data are not available at the lowest potential temperatures except in the coldest regions at middle and high latitudes during winter.

commences in June in the lower stratosphere [e.g., *Tabazadeh et al.*, 2000], descent of denitrified air from above also contributes to the low values of HNO_3 in the lower reaches of the vortex.

3.1.2. September

[19] One month later in mid-September, descent is still ongoing (not shown) throughout most of the middle and high latitudes. Above ~ 400 K, HNO_3 depletion has intensified slightly in the vortex core, whereas abundances have risen near the vortex edge. Such increases are consistent with previous studies showing that HNO_3 recovery commences in midwinter [e.g., *Santee et al.*, 1999; *McDonald et al.*, 2000], even though temperatures remain below PSC formation thresholds in much of the vortex. *Santee et al.* [1999] attributed the increase in lower stratospheric HNO_3 over the August–September period to a combination of factors, including intermittent evaporation of local PSCs, vertical transport, and horizontal mixing. Unlike at higher altitudes, HNO_3 mixing ratios in the lowermost vortex and subvortex have decreased substantially from mid-August to mid-September. Using zonal mean H_2O and HNO_3 abundances from MLS to estimate the formation threshold for nitric acid trihydrate (NAT) PSCs [*Hanson and Mauersberger*, 1988], we find that temperatures on this day are below the NAT threshold in most of the southern polar region at 147 hPa (corresponding approximately to 12 km or 370 K), and are at or slightly below the NAT threshold in the vortex core at 215 hPa (~ 10 km, 340 K). Moreover, spaceborne lidar observations from CALIPSO indicate PSC formation in the ~ 12 to 15 km altitude range from June through early October in 2006 [*Pitts et al.*, 2009]. (Note that CALIPSO PSC detections are cut off at altitudes less than 4 km above the local tropopause to avoid cirrus contamination.) Thus the decrease in gas-phase HNO_3 observed in the subvortex in mid-September is likely associated with ongoing PSC activity.

[20] Between mid-August and mid-September, ozone has become substantially depleted at polar latitudes throughout the vertical range shown. It has been suggested that apparent deficits in ozone revealed by tracer correlations at and below the bottom of the vortex have arisen through subsidence of ozone-depleted air from the vortex above [*Proffitt et al.*, 1993; *Collins et al.*, 1993; *Bregman et al.*, 1995]; although those studies focused on the Arctic, such effects could occur in the Antarctic as well. Similarly, *Bregman et al.* [2000] used in situ tracer correlation slope distributions and modeling to illustrate that, depending on the strength and longevity of the winter polar vortex, unmixed air transported below the bottom of the vortex by diabatic descent directly influences air in the Arctic LMS as far down as 340 K. On the other hand, *Murphy* [1991] calculated large chlorine-catalyzed ozone loss rates in the 350–400 K region over Antarctica based on in situ aircraft measurements of ClO in late August and September during the 1987 AAOE campaign. More recently, modeling results of *Lee et al.* [2002] indicated that low O_3 values in the Antarctic subvortex (defined by them to be the region below 390 K) largely occur through in situ chemical destruction rather than descent of ozone-depleted air from the vortex proper.

[21] Local chemical ozone loss requires the presence of reactive chlorine. In situ measurements of ClO were obtained in the lowermost vortex from the ER-2 during AAOE

[*Anderson et al.*, 1989; *Brune et al.*, 1989]. Although most flight time was spent at higher potential temperatures in the lower stratosphere, on each flight a dive executed at the southernmost penetration into the vortex, typically near 72°S latitude, allowed construction of vertical profiles. These dive segments revealed ClO mixing ratios of ~ 0.1 ppbv at 350 K and 0.2–0.3 ppbv at 370 K, significantly enhanced over typical midlatitude values at these levels [*Anderson et al.*, 1989; *Brune et al.*, 1989]. *Lee et al.* [2002] noted that because of the rapidity of chlorine deactivation at subvortex altitudes, ClO is unlikely to become enhanced there through diabatic descent of activated air from the vortex. They relied on modeling results, historical PSC observations, and previously published coarse vertical resolution ground-based ClO measurements [*Solomon et al.*, 2000] to infer the occurrence of significant chlorine activation at subvortex altitudes, with model values of reactive chlorine exceeding 0.5 ppbv at 350–380 K in mid-August to mid-September.

[22] As mentioned above, MLS and CALIPSO data indicate persistent PSC formation in the lowermost vortex at this time. Consistent with the presence of PSCs, MLS measurements (Figure 3) show that in middle to late winter HCl is depleted and ClO is enhanced inside and below the region of strong PV gradients defining the edge of the vortex proper. These measurements constitute the first simultaneous observations of HCl and ClO covering much of the Antarctic lowermost vortex and subvortex and provide direct evidence that substantial chlorine activation is widespread in this region. The altitude of maximum lower stratospheric ClO enhancement decreases progressively throughout the winter, following the patterns in temperature and thus PSC formation [*de Zafra et al.*, 1995; *Solomon et al.*, 2002; *Santee et al.*, 2003, 2008b]; from Figure 3 it is seen that the greatest enhancement in the lowermost vortex and subvortex is reached in mid-September. Observed maximum EqL-mean ClO abundances in the subvortex (~ 0.6 ppbv) are in line with those predicted in the modeling study of *Lee et al.* [2002] and are slightly larger than those measured by the ER-2 [*Anderson et al.*, 1989; *Brune et al.*, 1989].

3.1.3. October

[23] By mid-October, the polar vortex extends down to ~ 350 K (Figures 2 and 3). The downward extension of the vortex transport barrier over the August–October 2006 interval is consistent with the calculations of *Haynes and Shuckburgh* [2000b] and *Manney et al.* [1994]. Ozone is severely depleted throughout the vortex/subvortex region. As will be discussed further below, more ozone loss has taken place in the LMS in this year than in other years observed by Aura MLS. Chlorine activation is also more prolonged in 2006. Figure 3 shows that, although deactivation is underway by the beginning of the month (note the strong correlation between areas of high HCl and low ClO in the lowermost vortex core on 1 October), nonnegligible amounts of ClO are still evident in these EqL-mean cross sections at the bottom of the vortex at the end of the month. Because of the longer duration of active chlorine and the greater degree of ozone loss at lower altitudes, where it has a strong impact on the total column [e.g., *Rex et al.*, 2006], the 2006 ozone hole equals or exceeds records for both areal extent and ozone mass deficit [*World Meteorological Organization*, 2007b]. With chlorine substantially deactivated in most of the vortex by the end of October, however, ozone loss is curtailed for the most part.

Consistent with the chlorine deactivation, CALIPSO data indicate that PSCs have largely dissipated by the middle of the month [Pitts *et al.*, 2009]. HNO_3 mixing ratios have recovered substantially throughout the lowermost vortex/subvortex (Figure 2), most likely through release from PSCs either formed at those levels or deposited there via sedimentation from above. Such renitrification through evaporation of falling PSCs has been observed around the 12-km level in the late winter in both the Antarctic [Hofmann and Deshler, 1991] and the Arctic [e.g., Hübner *et al.*, 1990; Fischer *et al.*, 1997; Arnold *et al.*, 1998; Kondo *et al.*, 2000; Irie *et al.*, 2001; Koike *et al.*, 2002; Dibb *et al.*, 2006].

3.1.4. November

[24] Figures 2 and 3 show that in late October through mid-November, the lower part of the stratospheric polar night jet connects in an EqL-mean sense (i.e., at most longitudes) with an upper tropospheric jet, providing a single strong transport barrier over the entire altitude range depicted, as seen also by Haynes and Shuckburgh [2000b]. Manney *et al.* [2011] show, however, that in the LMS this transport barrier is not uniform with longitude; in some sectors (e.g., from roughly -170° to -80° longitude on 15 November), the extratropical tropopause is colocated with a strong subtropical upper tropospheric jet far equatorward of the polar jet/stratospheric jet complex, with moderate mixing in the broad latitude region between the subvortex edge and the tropopause.

[25] Interestingly, ozone has started to recover by this time. Small increases in ozone in the LMS between October and November are also seen in monthly mean ozonesonde profiles from southern high-latitude sonde stations [Logan, 1999]. High southern latitudes experience continuous sunlight starting in October. While the returning sunlight initiates photochemical production leading to a maximum in ozone abundances during spring and summer in the upper troposphere [e.g., Krebsbach *et al.*, 2006, and references therein], it also accelerates natural homogeneous gas-phase catalytic ozone destruction cycles in the stratosphere [e.g., Farman *et al.*, 1985; Perliski *et al.*, 1989; Brihl *et al.*, 1998; Fahey and Ravishankara, 1999]. Hegglin *et al.* [2006] used in situ measurements in the LMS over Europe to determine the altitude at which the chemical regime switches from net ozone production to net ozone destruction as a function of season. They found that in spring and summer, although ozone production takes place near the local tropopause, at altitudes higher than about 20 K above the tropopause, ozone destruction occurs, especially in the northern polar regions. Assuming similar behavior at southern high latitudes, the increase in ozone in the LMS observed between October and November in Figure 2 is unlikely to be solely attributable to net photochemical production. Likewise, because of the relatively strong transport barrier associated with the jet complex, horizontal mixing with extravortex air masses is also unlikely to account for much of the increase. Three-dimensional trajectory calculations driven by GEOS-5 analyses (not shown) indicate that by mid-November weak ascent is occurring above 370 K in the vortex/subvortex core, outside of which is a broad region of weak net descent. Thus the ozone distribution at this time is determined by different combinations of factors in different altitude and latitude domains, with vertical transport of higher O_3 abundances from either above or below, depending on the location, along

with horizontal mixing within the vortex between the edge and core regions (as exemplified in Figure 1).

[26] Turning to HNO_3 , at most altitudes values have continued to rebound from the lows observed in the vortex earlier in the winter (Figure 2), but they still remain depressed in mid-November. Because PSCs are probably no longer present at this time (well after the end of the typical Antarctic PSC season [Fromm *et al.*, 1997; Pitts *et al.*, 2009]), the residual depletion in HNO_3 implies the occurrence of permanent denitrification in the lower stratospheric vortex and subvortex. Denitrification has been observed down to 340 K in aircraft measurements [Fahey *et al.*, 1989]. The denitrified air is confined to EqLs poleward of $50\text{--}60^\circ\text{S}$ at all altitudes, even in the subvortex region.

3.1.5. December

[27] The polar vortex, though exceptionally long-lived in 2006 [World Meteorological Organization, 2007b], has begun to erode by mid-December (as evidenced by the PV gradients). The signatures of denitrification and ozone loss have been substantially diluted. The flattening of the trace gas contours seen in Figure 2 suggests that efficient exchange between polar (formerly inner vortex) and midlatitude air masses has occurred throughout the LMS, consistent with previous results on the dispersal of vortex air to midlatitudes [e.g., Chen *et al.*, 1994; Waugh *et al.*, 1997; Haynes and Shuckburgh, 2000a].

3.1.6. January

[28] Between mid-December 2006 and mid-January 2007, the polar vortex has dissipated completely, and a transition has taken place from the vortex representing the major transport barrier to the subtropical jet/tropopause representing the major transport barrier in the LMS. With the disintegration of the vortex, chemically processed air is no longer confined to high latitudes, nor is unperturbed air excluded; mixing of polar and lower-latitude air can be seen in the near-total homogenization of the trace gas fields. The differences between the latitudinal tracer gradients at the highest and the lowest altitudes depicted in Figure 2 suggest that the transport in the lower stratosphere differs from that in the LMS following the breakup of the polar vortex. Similarly, modeling studies of the Arctic late spring/summer have found that, unlike at higher levels where substantial transport into the subtropics occurs, below $\sim 420\text{--}450$ K the top of the tropospheric subtropical jet inhibits the meridional propagation of vortex remnants, keeping ozone-depleted air confined poleward of approximately 55°N [Piani *et al.*, 2002; Konopka *et al.*, 2003]. For stratospheric tracers such as O_3 and HNO_3 , which generally have small abundances at these altitudes, mixing with depleted air from the vortex/subvortex leads to uniformly low values throughout the LMS. Export of polar-processed and ozone-depleted air from the decaying vortex is discussed in more detail in a subsequent section.

3.2. Interannual Variability

[29] To investigate interannual variability in polar processing in the lowermost vortex and subvortex, we show in Figures 4 and 5 plots for 2005/2006 like those discussed above; other Antarctic winter/spring periods observed by Aura MLS were also examined. Although depletion in gas-phase HNO_3 is typically more severe and extensive in mid-August, HNO_3 has recovered to a substantially greater degree by mid-September in 2005 (and in all other years, not

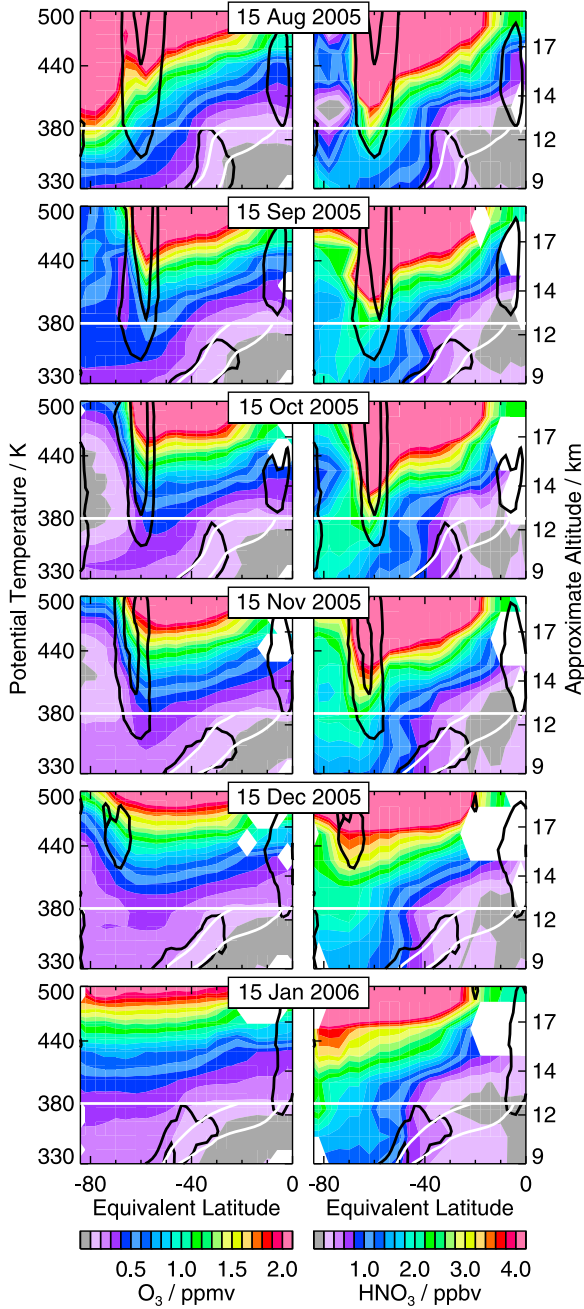


Figure 4. Same as Figure 2 except for the same calendar dates in 2005/2006.

shown) than in 2006 (compare Figures 2 and 4). Stronger descent throughout the extratropics (as indicated by the GEOS-5 diabatic heating rates, not shown) may have led to greater replenishment with higher- HNO_3 air from above in those years. In general, denitrification (as diagnosed by the persistent depression in gas-phase HNO_3 in mid-November) is weaker in all other years than in 2006, although November 2008 and 2009 (not shown) are also characterized by lingering low HNO_3 in the lowermost vortex. ClO is enhanced well into the subvortex in all years, with maximum enhancement below 400 K reached in mid-September, but the largest abundances extend to slightly lower altitudes in 2006 than in the other years (e.g., compare Figures 3 and 5).

Deactivation follows rapidly. Although vestiges of high ClO typically remain in parts of the lowermost vortex at the end of October, they disappear by mid-November in most years (not shown), with HCl abundances high throughout the region. Consistent with the shallower extent of active chlorine, the data suggest that less ozone has been destroyed in the lowermost vortex in the other years than in 2006 (compare Figures 2 and 4). The breakdown of the vortex occurs much earlier in 2005/2006 than in 2006/2007; in contrast, as in 2006, a relatively strong vortex persists in mid-December in 2007, 2008, and 2009 (not shown). In all years, the trace gas fields are almost fully homogenized by mid-January. Thus, although specific details vary from year to year, the overall

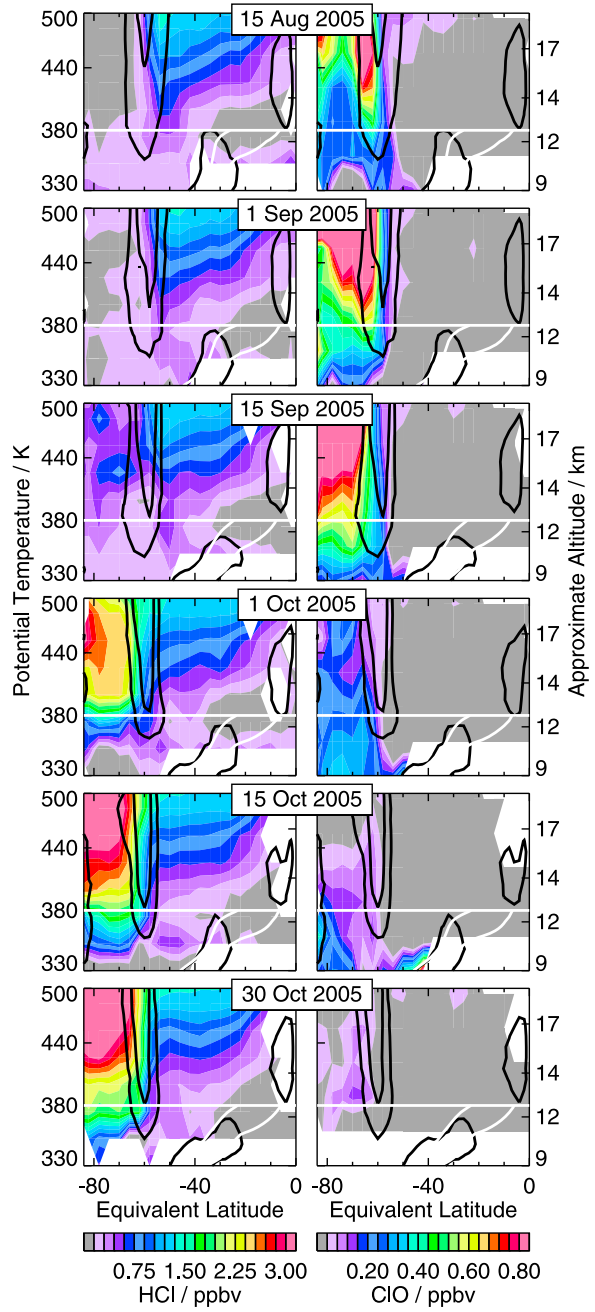


Figure 5. Same as Figure 3 except for the same calendar dates in 2005.

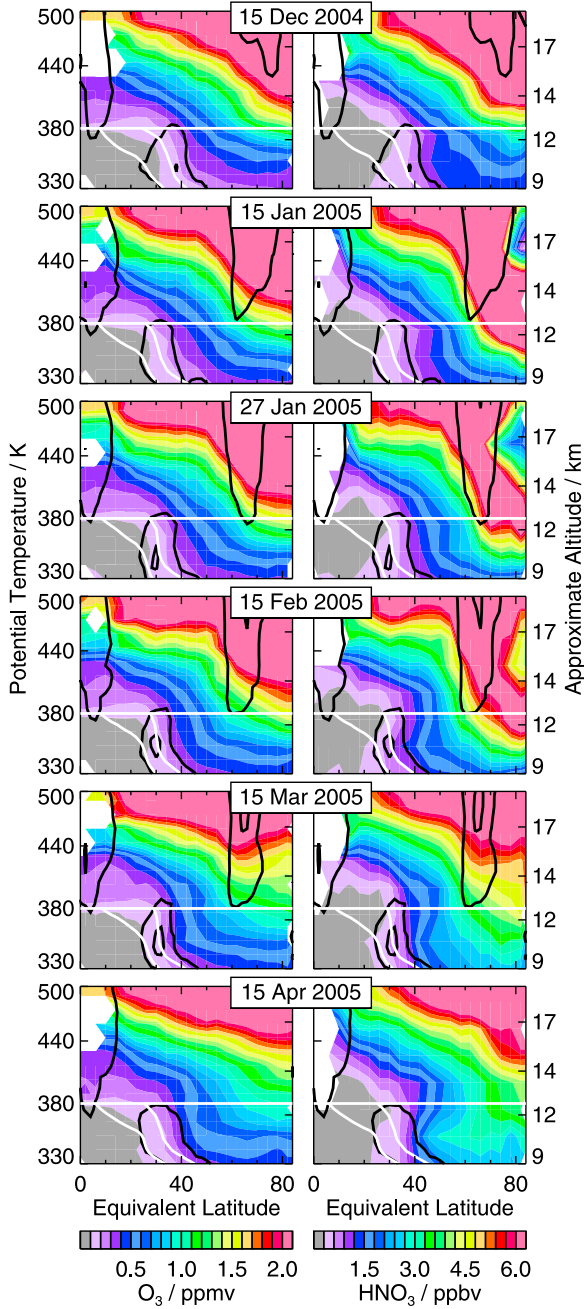


Figure 6. Same as Figure 2 except for the Northern Hemisphere 2004/2005 winter. Note that the contour increments for HNO₃ differ slightly from those used in the Southern Hemisphere.

dynamical and chemical behavior of the lowermost vortex and subvortex is qualitatively similar in all Antarctic winters observed so far by Aura MLS.

3.3. Northern Hemisphere Seasonal Variations

[30] Haynes and Shuckburgh [2000b] showed that the bottom of the Arctic vortex-edge barrier is weaker, descends less deeply into the LMS, and persists for a shorter duration than its Antarctic counterpart. The evolution of the Arctic vortex and subvortex is illustrated for the 2004/2005 winter in Figures 6 and 7. Much has already been written about the

chlorine activation, denitrification, and ozone loss observed during this exceptionally cold (for the Arctic) winter [e.g., World Meteorological Organization, 2007a; Santee *et al.*, 2008b, and references therein]. The early winter lower stratospheric vortex is characterized by slightly sharper PV

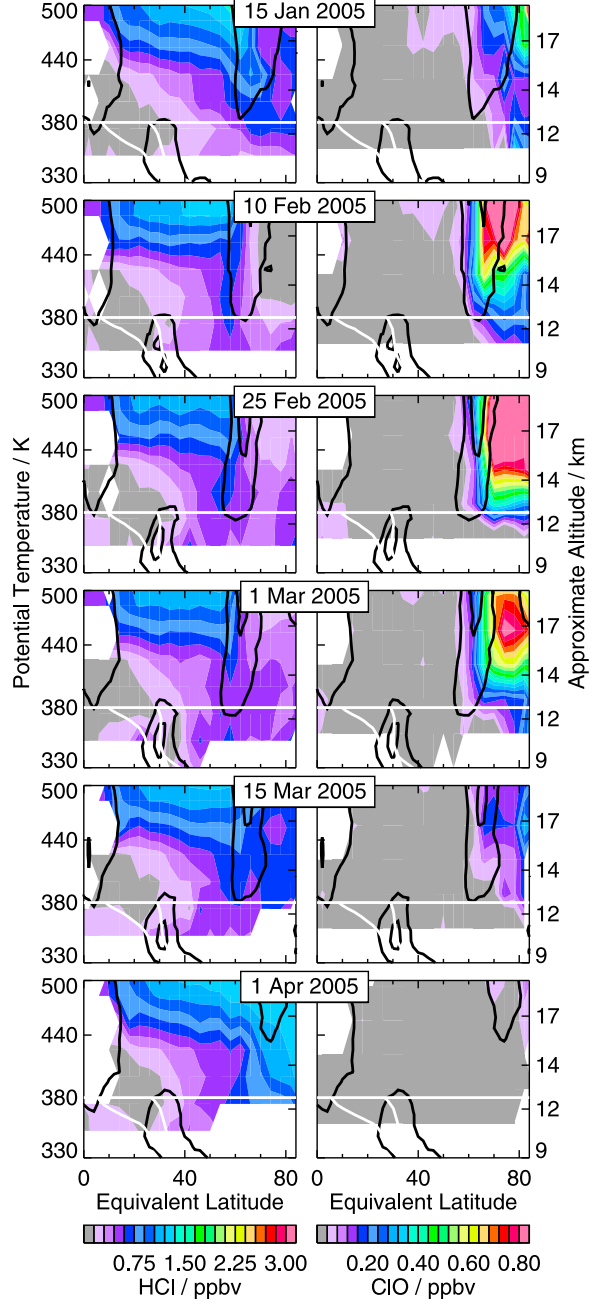


Figure 7. Same as Figure 3 except for the Northern Hemisphere 2004/2005 winter. As for the Southern Hemisphere, different dates are shown for HCl and ClO than for O₃ and HNO₃ to more closely track the progression of chlorine activation/deactivation. Note that because a particular potential temperature surface corresponds to a higher pressure under warmer conditions, the abundances of HCl and ClO, which are not retrieved at pressures larger than 147 hPa, do not extend as far into the subvortex region in northern midwinter as they do in southern midwinter (Figure 3).

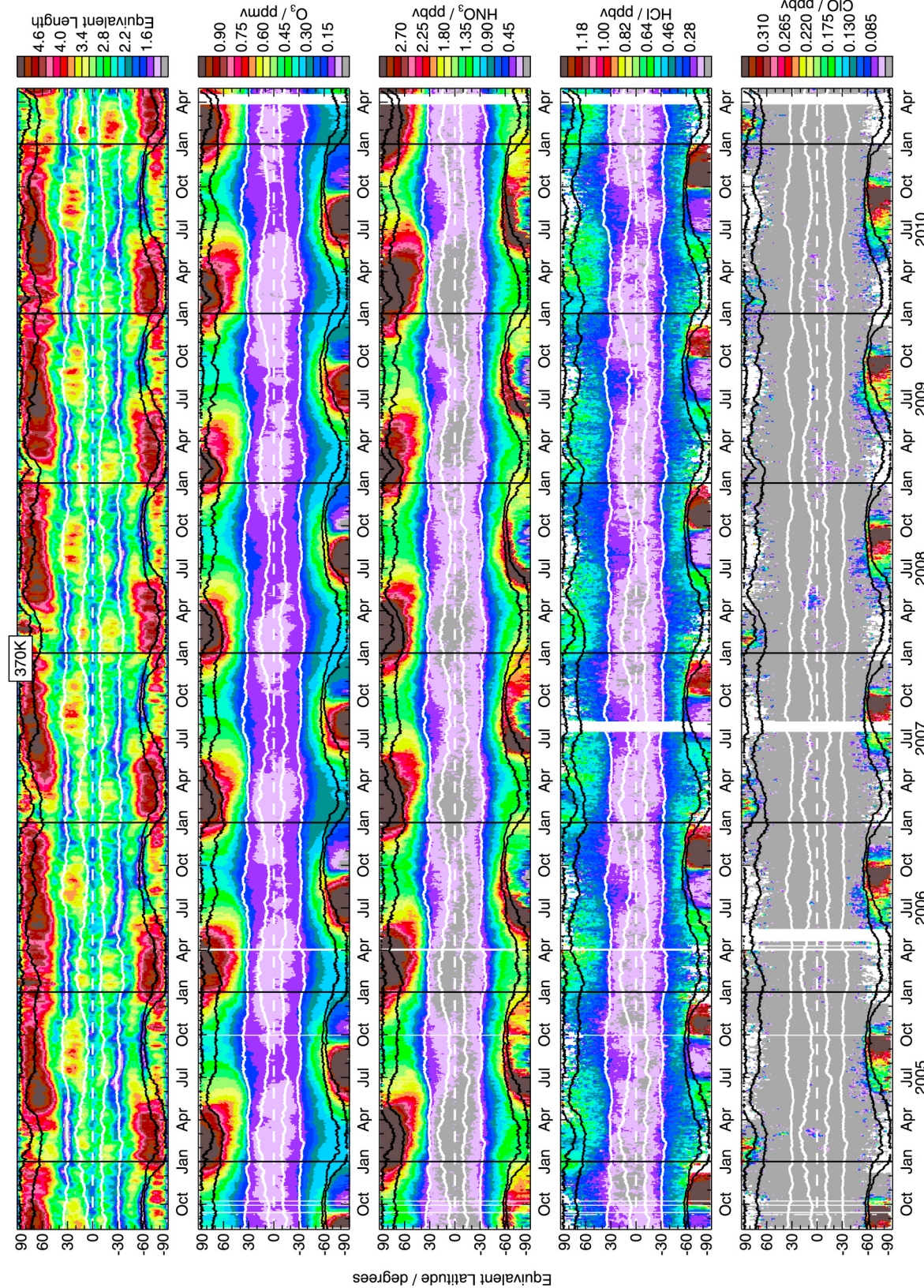


Figure 8

gradients and stronger descent than average, and the December 2004 fields reflect the seasonal buildup in O₃ and HNO₃. The significant depression in gas-phase HNO₃ visible at stratospheric levels at the highest EqLs in mid-January 2005 is a marker of PSC activity. Note that the gridding procedure used to produce the EqL/θ cross sections tends to smear out highly localized phenomena such as small-scale PSC events evident in daily maps (not shown), so PSC formation is likely to be more extensive than suggested by these panels. Very low temperatures are reached over a broad area in the lower stratosphere in late January, triggering formation of water ice PSCs in a dehydration event captured by MLS [Jimenez et al., 2006]. Figure 6 shows that HNO₃ is also severely depleted in the stratospheric vortex at this time. Although temperatures in the lowermost vortex and subvortex remain at or above NAT PSC formation thresholds (calculated based on zonal mean MLS HNO₃ and H₂O mixing ratios) even during the cold interval in late January, HNO₃ at these levels is seen to decrease slightly from its values earlier in the month. The effects of extant PSCs or denitrification (or both) continue to suppress gas-phase HNO₃ abundances in the stratospheric vortex core in mid-February. Analyses of both aircraft and satellite measurements have established the occurrence of substantial (though spatially inhomogeneous) denitrification in this winter [Kleinböhl et al., 2005; Jin et al., 2006; Schoeberl et al., 2006], as well as renitification at lower altitudes from the evaporation of PSCs sedimenting from above [Dibb et al., 2006; Jin et al., 2006]. The signature of individual renitification events is largely obliterated in the EqL-mean cross sections of Figure 6, however.

[31] Brune et al. [1990] compared the ClO profile obtained from the ER-2 on a dive inside the Arctic vortex in February 1989 to one obtained on a similar dive inside the Antarctic vortex in August 1987. As in the Antarctic, ClO mixing ratios were found to be ~100 times larger than typical midlatitude abundances at all altitudes, with the profiles from the two hemispheres in excellent agreement above ~400 K. Consistent with this picture, measurements from the previous MLS instrument onboard the Upper Atmosphere Research Satellite (UARS) also showed that enhanced ClO abundances comparable to those observed over Antarctica are attained at some levels in the Arctic lower stratosphere [Waters et al., 1993; Santee et al., 2003]. Brune et al. [1990] concluded, however, that ClO abundances decrease more rapidly at lower potential temperatures in the Arctic than in the Antarctic, attributing the difference to the fact that the vertical extent of PSC formation generally does not reach to as low altitudes in the Arctic. Comparison of Figures 3 and 5 with Figure 7 substantiates the finding that strong ClO enhancement (which peaks in

mid-February in 2005) does not extend as deeply into the subvortex region in the Arctic as it does in the Antarctic, even considering that the vortex/subvortex transition occurs at higher altitudes in the Arctic. This is true even for the 2004/2005 winter, during which the vortex was anomalously cold, especially below 400 K [Rex et al., 2006]. Nevertheless, the enhanced ClO (exceeding 0.2 ppbv) and depleted HCl evident in the EqL-mean cross sections of Figure 7 demonstrate that significant chlorine activation can occur down to and below 380 K in the Arctic.

[32] Consistent with the extensive area of extremely low temperatures and chlorine activation below 400 K, chemical ozone losses are larger in this region in 2005 than in other Arctic winters, leading to record depletion of column ozone by March 2005 [Rex et al., 2006; World Meteorological Organization, 2007a]. Although this loss is partially offset by replenishment through dynamical processes (which must be rigorously accounted for to accurately quantify the chemical destruction), some signature of it is evident in the change in the high-latitude ozone gradients between mid-February and mid-March in Figure 6.

[33] Although a major final warming halted PSC processing in early March [e.g., World Meteorological Organization 2007a], a strong transport barrier associated with the polar night jet is still identifiable in the middle of the month, and ClO mixing ratios are still slightly elevated (Figure 7). By the beginning of April, chlorine deactivation is complete. HCl abundances, however, remain relatively low throughout the vortex/subvortex. The different pattern of HCl behavior at the end of the winter in the north compared to that in the south (compare Figures 3, 5, and 7) is a consequence of the fundamentally different chlorine deactivation pathways in the two hemispheres, with reformation of ClONO₂ playing a much greater role in the Arctic [e.g., World Meteorological Organization, 2007a; Santee et al., 2008b, and references therein]. The vortex has broken down completely by mid-April (Figure 6), and, as discussed in connection with the Antarctic, the subtropical jet/tropopause has become the dominant transport barrier, with the flattening of the trace gas contours in the lower and lowermost stratosphere reflecting the homogenization of the fields.

4. Temporal Evolution of Trace Gases and Transport Barriers in the Lowermost Stratosphere

[34] The power of the satellite data record, with multiple years of daily global measurements, is more fully exploited by examining time series. Figures 8 and 9 show nearly seven years of MLS measurements at, respectively, 370 K and

Figure 8. EqL-time series at 370 K of effective diffusivity (κ_{eff} , expressed as lognormalized equivalent length) calculated from GEOS-5 Modern Era Retrospective-analysis for Research and Applications (MERRA) PV, and MLS O₃, HNO₃, HCl, and ClO. White contours show the 1.5 and 4.5 PVU values to mark the tropopause. Black contours represent the GEOS-5 1.2 and $1.4 \times 10^{-4} \text{ s}^{-1}$ sPV values to demarcate the polar vortex boundary; as in Figure 1, two contours are shown to indicate its strength. The vertical black solid lines denote year boundaries, and the horizontal white dashed line marks the equator. Blank spaces indicate missing data. Note that 370 K corresponds approximately to 150 hPa or ~12 km in much of the extratropics, but closer to 100–120 hPa or even lower pressures in the winter polar regions and the tropics; in the high temperatures of polar summer, the 370-K surface for the most part lies below the lowest level at which HCl and ClO are retrieved (147 hPa). Elevated ClO abundances intermittently present in the tropics do not represent real signatures of chlorine activation; see the discussion of similar artifacts at midlatitudes in section 4.1.

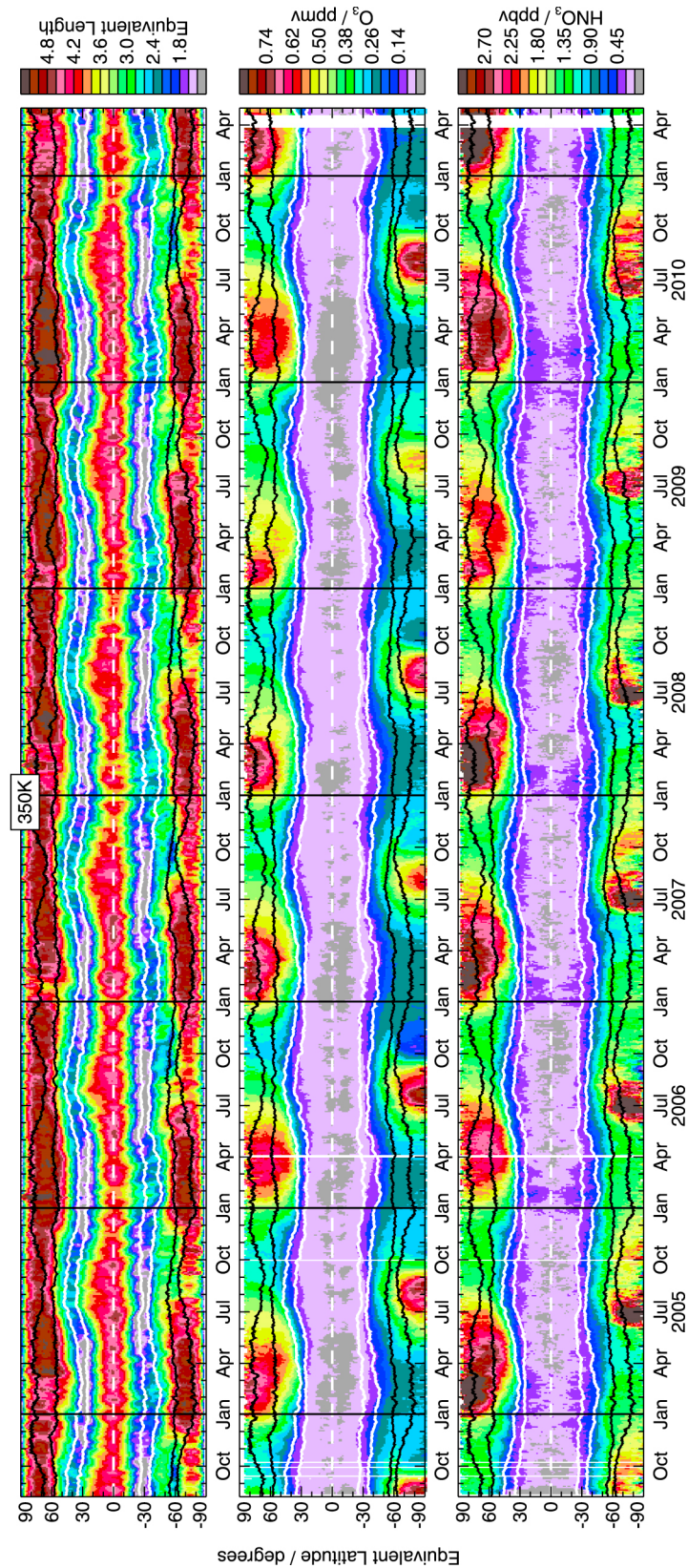


Figure 9. Same as Figure 8 except for 350 K. Note that 350 K corresponds approximately to 180 hPa or ~11 km in much of the extratropics, but closer to 130–150 hPa or even lower pressures in the winter polar regions; except for inside the Antarctic winter polar vortex, the 350-K surface lies below the lowest level at which HCl and ClO are retrieved, and consequently they are omitted from this plot.

350 K. These EqL/time plots are produced in a manner similar to that for Figures 2–7, but are gridded in time (grid points at 1200 UT each day) rather than potential temperature [Manney *et al.*, 2007]. As in previous figures, white and black contours demarcate the tropopause and the edges of the polar vortices, respectively.

[35] To gain insight into the seasonal and interannual variations in the strength of mixing barriers and their effect on trace gas distributions, MLS measurements are compared to effective diffusivity, κ_{eff} , calculated from analyzed PV. κ_{eff} provides a measure of the length of a tracer contour with respect to the minimum length that would enclose the same area; it thus tends to be relatively large (small) in regions of strong (weak) mixing, where the geometric structure of tracer contours is complex (simple) [Nakamura, 1996; Haynes and Shuckburgh, 2000a; Allen and Nakamura, 2001]. It can therefore be used to characterize the strength of transport barriers. Although κ_{eff} calculated directly from PV is noisier than that calculated using the advection-diffusion model of Allen and Nakamura [2001] (especially in regions of strong mixing), our analyses show that the two approaches produce qualitatively consistent fields.

[36] We begin with 370 K (Figure 8), which, at least in the Southern Hemisphere, is near the vortex/subvortex transition. The low values of κ_{eff} coincident with the white contours near 30° in each hemisphere mark the subtropical jet/tropopause transport barrier. The robustness of the tropopause barrier varies over the annual cycle; in both hemispheres it is substantially weakened during the summer by monsoon mixing [e.g., Haynes and Shuckburgh, 2000b; Scott *et al.*, 2003]. All fields shown exhibit a pronounced seasonal cycle at middle and high EqLs, controlled by the seasonality of the downward mass flux from above into the LMS as well as this region's isolation from the troposphere [e.g., Hegglin *et al.*, 2006], both of which are greatest in winter [e.g., Bönisch *et al.*, 2009].

4.1. Southern Hemisphere Extratropics at 370 K

[37] Quasi-confined diabatic descent inside the strengthening Antarctic polar vortex leads to a buildup in O₃, HNO₃, and HCl at this level in late fall and early winter (May–June). By midwinter (July), strong sPV gradients and low κ_{eff} values characterize the boundary of the lowermost vortex; although by no means impermeable, the vortex “edge” at this level does provide a significant barrier to meridional exchange of material between middle and high latitudes. Severe depletion in gas-phase HNO₃ is associated with PSC formation and/or denitrification. As a consequence of heterogeneous processing on PSCs and other cold aerosol particles, strong chlorine activation occurs, as evidenced by very low HCl and enhanced ClO inside the winter polar vortex. The MLS data appear to indicate the occasional occurrence of extravortex ClO enhancement as well. On the basis of model simulations, Lee *et al.* [2002] concluded that chlorine is efficiently deactivated at the boundary of the chemically perturbed region and thus does not remain significantly elevated in air that is exported from the subvortex to midlatitudes. A previous modeling study had also found that ClO enhancements arising from transport of polar-processed air are limited in geographical and temporal extent and would not generally be observed at middle latitudes in the stratosphere [Douglass *et al.*, 1991]. Therefore the apparent

ClO enhancements in the southern midlatitudes (outside of the polar vortex) from April or May through August every year are more likely to be an artifact in the MLS data attributable to imperfect ClO bias correction (which is performed on pressure surfaces before the data are interpolated to potential temperature, and thus can lead to time-varying effects as the relationship between pressure and potential temperature changes with ambient temperature) or cloud contamination (see section 2) than to be indicative of either leakage of chlorine-activated air from the vortex or in situ chlorine activation on extravortex PSCs or other aerosols.

[38] Rapid ozone loss commences in late August or early September. Minimum O₃ values in the lowermost vortex core are reached in October. The much greater degree of ozone loss in the Antarctic LMS in 2006 than in the other years observed so far by Aura is clearly evident in Figure 8, consistent with the greater extent and duration of ClO enhancement in that year. October ozone abundances are also unusually low in 2008, when the ozone hole area and mass deficit are second only to 2006 for the years since the Aura launch [World Meteorological Organization, 2008]. By the end of October, O₃ starts to rebound slightly throughout the vortex, most likely through a combination of transport processes as discussed in section 3.1.

[39] Like ozone, HNO₃ generally starts to show signs of recovery in October, but it remains strikingly low at this level in October–December in 2006 and 2008 (and also 2009). In the case of HNO₃, interannual variability may arise in part from differences in the magnitude of renitrification through evaporation of either in situ or sedimenting PSCs; counteracting this recovery, returning sunlight initiates photolytic loss of HNO₃ beginning in October. Although for the most part ClO declines in a similar manner at the end of every winter, interannual variability is seen in the reformation of HCl, which increases rapidly throughout the vortex in late September/early October. HCl eventually rises to values considerably above those observed by MLS before the onset of chemical processing at the beginning of winter, as noted previously for stratospheric altitudes by Santee *et al.* [2008b]. Larger HCl mixing ratios are attained over a greater area in October 2006 and 2008 than in the other years. This pattern is consistent with the smaller ozone abundances in 2006 and 2008, as modeling studies (for the lower stratosphere) have shown that HCl production is highly favored under conditions of severe ozone loss, and even slight differences in ozone levels can lead to significant differences in HCl values at the end of the winter [Douglass *et al.*, 1995; Groob *et al.*, 1997, 2005; Mickley *et al.*, 1997; Douglass and Kawa, 1999].

[40] In addition to chemical and microphysical processing during winter, dynamical factors, such as differences in transport and mixing, partially account for the observed springtime interannual variations. One source of dynamical variability in these species is the quasi-biennial oscillation (QBO) of the direction of the equatorial zonal wind in the stratosphere. Although the QBO is a tropical phenomenon, it exerts a significant influence on trace gas distributions in the extratropics through modulation of wave propagation and thus the circulation throughout the stratosphere (and even into the troposphere) [e.g., Baldwin *et al.*, 2001]. A QBO signal has previously been modeled and observed at middle and high latitudes in the lower stratosphere in several trace species, including O₃, HNO₃, and HCl [e.g., Chipperfield and

Gray, 1992; Baldwin *et al.*, 2001, and references therein], and, because of its strong impact on isentropic mixing, in κ_{eff} [Haynes and Shuckburgh, 2000a]. We note that tropical and northern midlatitude MLS H₂O mixing ratios in January–April are also much lower in 2006 and 2008 than in the other years (not shown), consistent with a QBO effect.

[41] Other processes affecting atmospheric temperature and circulation may also give rise to some of the interannual variations in these species. For example, the North Atlantic and Antarctic Oscillations, leading modes of variability for the climate of the Northern and Southern Hemispheres, respectively, alter the transport and mixing of chemical species into and out of the subvortex region [Shuckburgh *et al.*, 2009]. Finally, El Niño/Southern Oscillation (ENSO) influences polar processing in and the permeability and persistence of the winter polar vortex [e.g., Sassi *et al.*, 2004, and references therein]. In addition, the mixing barriers at the subtropical jets are stronger, more zonal, and shifted equatorward during the positive phase (El Niño years) [Scott *et al.*, 2003; Shuckburgh *et al.*, 2009]. However, visual inspection of Figure 8 uncovers no clear correlation between the observed trace gas variations and the occurrence of relatively strong El Niño or La Niña events during the Aura mission (based on the Niño 3.4 sea surface temperature index [e.g., Trenberth, 1997]), implying that the ENSO signal is weak and difficult to discern against the larger-amplitude seasonal and QBO cycles. Conclusive identification of these more subtle signatures in the MLS data would require detailed analyses beyond the scope of this paper and would also benefit from a longer data record.

[42] Breakup of the Antarctic vortex normally proceeds from the top down; it has been shown to typically reach altitudes slightly above the 370 K level of interest here in December [e.g., Zhou *et al.*, 2000; Haigh and Roscoe, 2009]. Even before the vortex has fully broken up, however, more erosion of vortex air takes place in late winter at this level than at higher altitudes in the lower stratosphere [e.g., Chen *et al.*, 1994]. The divergence of the sPV contours and the dramatic increase in κ_{eff} in Figure 8 signal the collapse of the transport barrier and subsequent strong mixing and exchange of air between high and middle latitudes, consistent with previous findings [e.g., Chen *et al.*, 1994; Waugh *et al.*, 1997; Haynes and Shuckburgh, 2000a]. The abrupt changes in the extravortex trace gas contours in November and December as sPV gradients weaken, particularly visible in O₃ and HCl, imply the export of processed air from the vortex. Although coherent fragments can drift from the eroding vortex, below 20 km these remnants lose their distinct vortex identity within a few weeks in the face of vigorous stirring [e.g., Konopka *et al.*, 2003; Manney *et al.*, 2005]; in any case, such small vortex shards would not be discernible in the EqL-mean cross sections shown here.

[43] Model studies have indicated that in situ midlatitude chemical ozone destruction induced by transport of enhanced-CIO air from the lower stratospheric vortex is limited [Prather and Jaffe, 1990; Douglass *et al.*, 1991; Norton and Chipperfield, 1995; Konopka *et al.*, 2003]. In contrast, the irreversible mixing of ozone-poor air from the decaying polar vortex at the end of the winter has been shown to have a significant impact on midlatitude ozone. Various studies have quantified this so-called “dilution” effect in both hemispheres, on timescales both seasonal (i.e., for individual

years) [Brasseur *et al.*, 1997; Knudsen and Grooß, 2000; Lee *et al.*, 2002; Marchand *et al.*, 2003; Millard *et al.*, 2003; Ajtic *et al.*, 2004] and multiannual (i.e., considering the accumulated effects resulting from successive bouts of polar ozone loss) [Sze *et al.*, 1989; Eckman *et al.*, 1996; Chipperfield, 1999, 2003; Fioletov and Shepherd, 2005; Yang *et al.*, 2006]. The fraction of observed midlatitude ozone reduction attributable to transport of polar ozone-depleted air was found to be as large as 40–50% in these analyses. In addition to the effects on ozone, a rough estimate of the efflux of dehydrated air from the Antarctic vortex between August and September has been made based on UARS Halogen Occultation Experiment measurements [Rosenlof *et al.*, 1997]. Other species, however, have rarely been discussed in this context; moreover, only the study of Lee *et al.* [2002] specifically focused on the LMS. Figure 8 shows that all of these trace gas fields are influenced by the dispersal of processed air from the Antarctic vortex and subvortex.

[44] A temporary slight weakening of the Southern Hemisphere subtropical jet/tropopause transport barrier occurs over the interval from about January through April (note the higher κ_{eff} values in Figure 8) [e.g., Haynes and Shuckburgh, 2000b; Scott *et al.*, 2003]. One of the unique aspects of the LMS is that isentropic surfaces intersect the tropopause in this region, allowing rapid quasi-horizontal stratosphere-to-troposphere and troposphere-to-stratosphere mass exchange to take place [e.g., Holton *et al.*, 1995; Shepherd, 2007]. Both modeling [e.g., Chen, 1995; Dethof *et al.*, 2000; Berthet *et al.*, 2007] and observational [e.g., Ray *et al.*, 1999; Hegglin *et al.*, 2006, 2009; Pittman *et al.*, 2007] studies have indicated the occurrence of substantial quasi-isentropic transport of tropical tropospheric air into the extratropical LMS in the summer hemisphere, associated with the planetary-scale anticyclonic circulations of the summer monsoons. Similarly, Bönisch *et al.* [2009] analyzed in situ aircraft observations and found that, although a significant amount of young tropospheric air can be observed at this level in all seasons (including spring and winter, as seen also by Spackman *et al.* [2007]), during summer and autumn the composition of the LMS is dominated by tropospheric air delivered in part via quasi-horizontal mixing across the subtropical tropopause; their results showed that transport from the tropical lowest stratosphere just above the tropopause with subsequent subsidence in the lower (shallow) branch of the summertime Brewer-Dobson circulation is also a major pathway for young tropospheric air into the LMS. The majority of the tropospheric fraction of air observed in the LMS originates from the tropics, whereas air from the local extratropical troposphere plays only a minor role in influencing the composition in the near-tropopause layer [e.g., Hoor *et al.*, 2005; Berthet *et al.*, 2007; Bönisch *et al.*, 2009].

[45] Consistent with this picture, the trace gas contours in Figure 8 also suggest summertime incursions of tropical air into the extratropics, as seen in the slightly smaller mixing ratios of all species in the region just poleward of the tropopause in every year. (Note that in addition to the strong seasonal variations, there is considerable interannual variability in isentropic cross-tropopause exchange [e.g., Seo and Bowman, 2001; Schoeberl, 2004].) Tropospheric air parcels are characterized by much lower ozone mixing ratios than stratospheric ones. Accordingly, some of the seasonal cycle seen in extratropical ozone in the LMS in Stratospheric

Aerosol and Gas (SAGE) II [Pan *et al.*, 1997; Wang *et al.*, 1998, 2006], Polar Ozone and Aerosol Measurement (POAM) III [Prados *et al.*, 2003], and airborne in situ [Krebsbach *et al.*, 2006; Heggen *et al.*, 2006] data has been attributed to summertime influx of ozone-poor tropospheric air. In addition to troposphere-to-stratosphere transport, some of the observed summertime decrease in lowermost stratospheric ozone (at northern midlatitudes) has been linked to changes in tropopause height [Prados *et al.*, 2003; Krebsbach *et al.*, 2006]. However, Wang *et al.* [2006] demonstrated that vertical displacement of the tropopause cannot by itself induce ozone variations large enough to explain the observed seasonal cycle in midlatitude ozone in the tropopause region. We thus conclude that the transient (roughly January through April) dip in Southern Hemisphere extratropical O₃ mixing ratios every year (Figure 8) is associated with cross-tropopause mixing of tropical tropospheric air into the LMS. Likewise, since HCl is a stratospheric tracer with no known sources of significance in the upper troposphere [Marcy *et al.*, 2004, 2007], transport and mixing of air from the tropical troposphere also leads to a reduction in HCl mixing ratios. The situation for HNO₃ is somewhat more complicated: Because of local sources (e.g., lightning) and sinks (e.g., cirrus clouds), HNO₃ abundances in the tropical upper troposphere are highly variable and can be comparable to those in the LMS [e.g., Murphy *et al.*, 1993; Popp *et al.*, 2009]. In general, however, HNO₃ values are considerably smaller in the tropical upper troposphere than in the LMS, so again in-mixing from the tropics would be expected to lead to seasonal decreases in extratropical HNO₃ at this level in the EqL-mean view of Figure 8.

[46] In addition to the influence of transport and mixing, chemical effects are at work in the summertime LMS. The late-summer/early-autumn minimum in middle and high latitude stratospheric ozone is a well-known feature [e.g., Bowman and Krueger, 1985; Froidevaux *et al.*, 1994; Park and Russell, 1994; Wang *et al.*, 1998] largely attributable to intensified photochemical destruction by radical (in particular NO_x) catalytic cycles in the continuous sunlight of polar day [e.g., Farman *et al.*, 1985; Perliski *et al.*, 1989; Brühl *et al.*, 1998; Fahey and Ravishankara, 1999], with little or no counterbalancing dynamical replenishment at this season. While summertime ozone destruction rates are considerably slower below 100 hPa than they are higher in the stratosphere, they are still nonnegligible [Brühl *et al.*, 1998], and a small amount of net photochemical removal takes place [Bregman *et al.*, 2001]. It is also possible that heterogeneous processing on cirrus clouds or aerosols, analogous to that on PSCs in the winter polar vortices, promotes chlorine-catalyzed ozone destruction in the LMS [McElroy and Salawitch, 1989; Solomon *et al.*, 1997; Lelieveld *et al.*, 1999; Hendricks *et al.*, 1999; Bregman *et al.*, 2002]; in the case of cirrus clouds, the impact on ozone may be largest near the midlatitude tropopause in summer (especially in the Northern Hemisphere) [Solomon *et al.*, 1997; Bregman *et al.*, 2002]. Similarly, during polar summer the slowing of vertical transport to this region combined with the uninterrupted illumination (which causes very low N₂O₅ concentrations [e.g., Farman *et al.*, 1985] and hence the cessation of N₂O₅ conversion into HNO₃, as well as photodissociation of HNO₃) also leads to low HNO₃, as reported previously for stratospheric altitudes [e.g., Santee *et al.*, 1999, and refer-

ences therein]. Although HCl, like O₃ and HNO₃, has a relatively long photochemical lifetime of the order of weeks in the UTLS [Marcy *et al.*, 2004], some degree of photochemical destruction of HCl may also occur at this level.

[47] The strong mixing (high κ_{eff} values) that is a hallmark of the summertime lower and lowermost stratosphere [e.g., Haynes and Shuckburgh, 2000a, 2000b; Scott *et al.*, 2003] eventually homogenizes the trace gas distributions throughout much of the extratropics, as noted earlier. Finally, by April or May descent inside the incipient Antarctic vortex begins once again to alter trace gas distributions at this level at middle and high EqLs, and the entire cycle repeats.

4.2. Northern Hemisphere Extratropics at 370 K

[48] Although the gross features of the distributions and annual cycles of the trace gases are very similar in both hemispheres in Figure 8, there are notable differences. The larger κ_{eff} values and weaker PV gradients reflect the much more permeable lowermost stratospheric vortex in the Arctic, where in most winters a barrier to transport barely exists at this level, as shown also by Haynes and Shuckburgh [2000b]. This is especially true during the highly dynamically disturbed winters of 2005/2006, 2008/2009, and 2009/2010, when major stratospheric sudden warmings prematurely terminated polar processing and prompted erosion of the vortex [Manney *et al.*, 2009a, 2009b; Lee *et al.*, 2011]; the greater degree of mixing out of the vortex during these winters is clearly evident, particularly in the O₃ and HNO₃ contours. Interhemispheric differences in wintertime diabatic descent rates [e.g., Manney *et al.*, 1994; Rosenlof, 1995], as well as the lack of an ozone “hole”, result in extratropical ozone abundances that are larger in the Northern Hemisphere than in the Southern Hemisphere over the entire annual cycle, as noted also in SAGE II measurements [Pan *et al.*, 1997; Wang *et al.*, 1998]. HNO₃ abundances are likewise larger throughout most of the northern extratropics than in the south, again through a combination of the stronger advection of HNO₃-rich air from above and the considerably smaller magnitude and extent of denitrification. In contrast, HCl is substantially lower in the Northern Hemisphere, where its seasonal cycle is weak. The modest degree of seasonal variation in HCl reflects not only the generally lesser amount of chemical processing inside the Arctic vortex/subvortex (evidence of which is particularly striking in the disparity in ClO enhancement in the two hemispheres), but also the fact that the dominant chlorine recovery pathway in the Arctic differs from that in the Antarctic, with reformation of ClONO₂ rather than HCl being the primary deactivation mechanism at the end of northern winter [e.g., World Meteorological Organization, 2007a; Santee *et al.*, 2008b, and references therein]. The substantial hemispheric asymmetry in the strength of troposphere-to-stratosphere transport, with greater influx of tropospheric air into the LMS during northern summer than during southern summer [e.g., Chen, 1995; Dethof *et al.*, 2000], also influences the extratropical distributions of all of these species at this level (especially visible in the HCl mixing ratios just poleward of the tropopause in this EqL-mean view).

4.3. Extratropics at 350 K

[49] The 350 K potential temperature surface lies in the subvortex region throughout the winter/spring periods in both

hemispheres and is thus a level of freer exchange between polar and midlatitude air masses. In fact, although a strong mixing barrier (modulated by the annual cycle) is present at the subtropical jets in each hemisphere, in the extratropics the κ_{eff} values and scaled PV gradients indicate a significant impediment to mixing only in the Southern Hemisphere in August through October (Figure 9). This is consistent with equivalent length calculations for the Antarctic winter and spring of 1996 reported by *Lee et al.* [2002], which indicated that the entire extratropical region on the 350-K surface was characterized by strong mixing. It is also in accord with the analyses at this level of effective diffusivity by *Haynes and Shuckburgh* [2000b] and a new diagnostic of transport and mixing termed Lyapunov diffusivity described by *Shuckburgh et al.* [2009]. Nevertheless, the MLS data clearly show the early winter buildup (in both hemispheres) and subsequent depletion (in the Antarctic) of high-latitude ozone. The extraordinary ozone loss in the 2006 Antarctic winter, discussed earlier, is even more striking at this level than it is at 370 K. In general, comparison of Figures 8 and 9 shows that both the amount of ozone and the amplitude of its seasonal cycle decrease with decreasing altitude, as expected for a constituent with its main source in the stratosphere and as reported previously in satellite [e.g., *Pan et al.*, 1997; *Prados et al.*, 2003] and airborne in situ [e.g., *Krebsbach et al.*, 2006] data. Very similar seasonal evolution is seen at ~350 K at lower latitudes in the SAGE II ozone climatology [*Wang et al.*, 2006]. Like O₃, HNO₃ exhibits patterns at 350 K very similar to those at 370 K, including interannual variation in the degree of Antarctic denitrification and recovery. Although for the most part the 350 K surface extends below the bottom of the range of useful HCl and ClO data, viable retrievals are obtained at this level in Antarctic winter (not shown in Figure 9). They suggest that chlorine is typically activated in the southern subvortex from early July through middle to late October, as noted previously in connection with Figures 3 and 5. As at 370 K, the signatures of polar processing start to be erased at the end of the winter, and the trace gas fields become more or less homogenized throughout the extratropics. Finally, in early summer in both hemispheres the tropopause transport barrier is seen to weaken and shift poleward (to ~50° EqL), consistent with the summertime poleward displacement of the subtropical jet [*Haynes and Shuckburgh*, 2000b; *Scott et al.*, 2003].

4.4. Tropics

[50] Because our primary focus in this study is chemical processing in and dispersal of chemically processed air from the lowermost vortex and subvortex, we have touched on the trace gas distributions in the tropics (where the seasonal variations in these species are generally much weaker) only insofar as they influence mixing ratios at higher latitudes. Particularly noteworthy, however, are the larger abundances of O₃, HNO₃, and HCl, more typical of the stratosphere, that encroach into the equatorial region at 370 K (Figure 8). Such patterns, visible in the Southern Hemisphere roughly from June or July until January or February every year, are signatures of stratosphere-to-troposphere transport. These recurring features often appear to “bridge” to stronger and deeper stratosphere-to-troposphere transport episodes in the Northern Hemisphere from April or May until October or November every year. The interhemispheric differences in

the strength and penetration of these cross-tropopause exchange events are more apparent in the HNO₃ and HCl distributions in Figure 8 than in ozone. The changes in the trace gas contours (and the interhemispheric asymmetry in them) are roughly correlated with increases in κ_{eff} during approximately the same intervals that largely occur between the two white contours bracketing the dynamical tropopause region in each hemisphere.

[51] Although the timing does not exactly match, the patterns of stratosphere-to-troposphere transport implied in Figure 8 are largely consistent with the results of *Haynes and Shuckburgh* [2000b], who found that above 350 K mixing is especially strong equatorward of the subtropical jet in June–September (December–March) in the Northern (Southern) Hemisphere. Their results indicated essentially no identifiable tropopause barrier at 370 K in summer in either hemisphere, which they attributed to monsoon-related mixing. Earlier, the modeling results of *Chen* [1995] showed that, in the upper portion of the LMS (350 K), stratosphere-to-troposphere transport is strongly inhibited during northern winter in the Northern Hemisphere, whereas a small amount of stratospheric tracer is transported into the troposphere at this time in the Southern Hemisphere and the Australian and South American summer monsoons act to further transport some fraction of that air into the northern subtropics. Correspondingly, the modeling study showed that during southern winter the tropopause represents a strong barrier to cross-tropopause transport in the Southern Hemisphere, whereas substantial stratosphere-to-troposphere transport occurs in the Northern Hemisphere at this time and the Asian and North American summer monsoons act to transport a significant amount of stratospheric tracer into the southern subtropics [*Chen*, 1995]. Evidence for possible isentropic cross-equatorial transport from the Southern to the Northern Hemisphere during southern summer and from the Northern to the Southern Hemisphere during northern summer has previously been seen in a climatological tropopause ozone distribution based on more than 20 years of SAGE II data [*Wang et al.*, 2006]. More recently, *Rogal et al.* [2010] used meteorological analyses, column ozone measurements, and modeling to show how cross-equatorial outflow from the Asian summer monsoon at 360 K influences the distribution of ozone in the Southern Hemisphere. Figure 8 reveals the signature of enhanced monsoon-related cross-equatorial transport in the distributions of HNO₃ and HCl as well as in ozone. That the summertime maximum in ozone in the tropics is apparently well-correlated with similar enhancements in stratospheric tracers such as HNO₃ and HCl has important implications for its origin. *Folkins et al.* [2006] and *Randel et al.* [2007] have argued that the large seasonal cycle in ozone near and just above the tropical tropopause, with highest values in boreal summer, primarily arises from seasonal changes in tropical upwelling and convective outflow. Both of those studies, however, assumed that mass exchange with the extratropics is negligible. In contrast, a recent analysis by *Konopka et al.* [2010] found that horizontal transport from the extratropics, mainly driven by the persistent monsoon anticyclones, substantially modulates tropical ozone between 370 and 420 K, with the strongest effects seen during late summer and early fall in the Northern Hemisphere. Our results support the notion that isentropic transport from the extratropics associated with the summer monsoons

significantly influences the composition of the tropical tropopause layer.

[52] Although still present to a limited extent (especially in HNO_3 during January through March), the signatures of stratosphere-to-troposphere transport are much less sharply defined in the MLS data at 350 K than at 370 K (compare Figures 8 and 9). The core of the subtropical jet is typically situated near 350 K, and consequently the tropopause transport barrier is stronger at that level [e.g., *Haynes and Shuckburgh, 2000b*], inhibiting cross-tropopause exchange to a greater extent there than at levels either above or below.

5. Summary and Synthesis

[53] Daily global measurements from Aura MLS have enabled the first comprehensive investigation of interhemispheric and interannual variations in chemical processing in and dispersal of processed air from the winter polar lowermost vortex and subvortex. Nearly seven years of MLS measurements of O_3 , HNO_3 , HCl and ClO are analyzed in conjunction with GMAO GEOS-5 meteorological data, including effective diffusivity calculated from PV as a measure of the strength of mixing barriers.

[54] Quasi-confined diabatic descent inside the incipient vortex leads to an early winter buildup in O_3 , HNO_3 , and HCl in the LMS. The MLS measurements reveal that, as in the vortex proper, extensive chemical processing takes place in the lowermost vortex and subvortex in both hemispheres. Indeed, the MLS data, which represent the first simultaneous observations of HCl and ClO throughout much of the LMS, provide direct evidence that chlorine activation is widespread in the subvortex in the Antarctic and can occur to a significant degree in this region in the Arctic as well. The 2006 Antarctic and 2004/2005 Arctic winters are highlighted here, as unusually low temperatures and relatively strong and prolonged chlorine activation in the lowermost vortex and subvortex promoted large ozone losses in those regions, consistent with reported record low column ozone in both of these winters. Although not quite as severe as that in 2006, the ozone destruction in the 2008 Antarctic winter subvortex also stands out. The larger ozone losses in these two Antarctic winters gave rise to larger springtime HCl mixing ratios, as HCl production is highly favored under low-ozone conditions. Interannual variability is also observed in the degree of denitrification and HNO_3 recovery in the Antarctic subvortex, with unusually low HNO_3 abundances seen in the spring of 2006 and 2008. These interannual variations may be linked to QBO or other dynamical effects. Dynamical factors play a large role in influencing the trace gas distributions in the Northern Hemisphere, where in most winters the lowermost vortex is much weaker, warmer, and shorter-lived and consequently chemical processing within it is much less intense than it is in the Southern Hemisphere. In particular, in the highly disturbed Arctic winters of 2005/2006, 2008/2009, and 2009/2010, major stratospheric sudden warmings resulted in enhanced mixing out of the eroded vortex.

[55] The breakdown of the vortex at the end of the winter triggers a transition from it functioning as the major transport barrier in the LMS to the subtropical jet/tropopause functioning as the major transport barrier. The influence of processed air mixing out from the decaying vortex/subvortex is clearly indicated by abrupt changes in the observed extra-

vortex trace gas contours at this time. With the weakening of the subtropical jet/tropopause transport barrier in summer, rapid quasi-isentropic transport of tropical tropospheric air into the extratropical LMS takes place, associated with the summer monsoon circulations. The MLS data show that such in-mixing from the tropical upper troposphere leads to seasonal decreases in the extratropical O_3 , HNO_3 , and HCl mixing ratios in the LMS in both hemispheres. The strong mixing that characterizes the summertime lower and lowermost stratosphere effectively homogenizes the trace gas fields throughout the extratropics. In addition, the MLS O_3 , HNO_3 , and HCl measurements in the tropics also show signatures of monsoon-related cross-equatorial stratosphere-to-troposphere transport.

[56] In summary, our results demonstrate that the concentrations of O_3 , HNO_3 , and HCl (and by extension other trace gases) in the extratropical LMS are controlled by the complex interplay between myriad chemical and dynamical processes. These processes include: large-scale air motions of the Brewer-Dobson circulation, and variations in it (such as QBO effects); local PSC formation, denitrification, renitrification, chlorine activation, and ozone destruction inside the winter polar lowermost vortex and subvortex; subsequent outmixing of processed air from the vortex/subvortex at the end of winter; and quasi-isentropic cross-tropopause transport and mixing with tropical and subtropical tropospheric air. Substantial interannual variability occurs in the meteorological conditions and consequently the extent and magnitude of chemical processing as well as the degree of confinement of processed air within the winter polar lowermost vortex and subvortex. In general, we find that the seasonal and interannual variations in the trace gas abundances in the LMS observed by Aura MLS are consistent with the evolution in the strength of the transport barriers as diagnosed from meteorological analyses.

[57] This study provides a broad overview of MLS trace gas observations in the LMS and draws inferences about the processes governing their distribution and variability. More detailed analyses are in progress and/or planned, including casting the MLS measurements into tropopause- and jet-based coordinate frameworks [e.g., *Manney et al., 2011*] to better elucidate transport and mixing processes in the extratropical tropopause region. Finally, we note that many of the processes described in this work, in particular those associated with stratosphere-troposphere exchange, have been diagnosed over limited spatial and temporal domains using in situ observations. While such measurements offer unparalleled insight into the instantaneous mechanisms affecting trace gas abundances in the LMS, the satellite measurements presented here afford a spatially and temporally integrated view, providing unique information on the large-scale “climatological” impacts of those pathways and underscoring the complementarity of the two observational approaches.

[58] **Acknowledgments.** We thank Ryan Fuller, William Daffer, Bob Thurstans, Brian Knosp, and Brian Mills for programming, system administration, and data management support. Helpful discussions with Alyn Lambert, Karen Rosenlof, Emily Shuckburgh, Sean Davis, Michaela Hegglin, Kent Minschwaner, and Doug Allen are greatly appreciated. Comments from three anonymous reviewers improved the manuscript. Work at the Jet Propulsion Laboratory, California Institute of Technology, was done under contract with NASA.

References

- Adriani, A., P. Massoli, G. Di Donfrancesco, F. Cairo, M. L. Moriconi, and M. Snels (2004), Climatology of polar stratospheric clouds based on lidar observations from 1993 to 2001 over McMurdo Station, Antarctica, *J. Geophys. Res.*, **109**, D24211, doi:10.1029/2004JD004800.
- Ajtíć, J., B. J. Connor, B. N. Lawrence, G. E. Bodeker, K. W. Hoppel, J. E. Rosenfield, and D. N. Heuff (2004), Dilution of the Antarctic ozone hole into southern midlatitudes, 1998–2000, *J. Geophys. Res.*, **109**, D17107, doi:10.1029/2003JD004500.
- Allen, D. R., and N. Nakamura (2001), A seasonal climatology of effective diffusivity in the stratosphere, *J. Geophys. Res.*, **106**, 7917–7935.
- Anderson, J. G., W. H. Brune, and M. H. Proffitt (1989), Ozone destruction by chlorine radicals within the Antarctic vortex: The spatial and temporal evolution of ClO-O₃ anticorrelation based on in situ ER-2 data, *J. Geophys. Res.*, **94**, 11,465–11,479.
- Appenzeller, C., J. R. Holton, and K. H. Rosenlof (1996), Seasonal variation of mass transport across the tropopause, *J. Geophys. Res.*, **101**, 15,071–15,078.
- Arnold, F., V. Bürger, K. Gollinger, M. Roncossek, J. Schneider, and S. Sprung (1998), Observations of nitric acid perturbations in the winter Arctic stratosphere: Evidence for PSC sedimentation, *J. Atmos. Chem.*, **30**, 49–59.
- Avallone, L. M., D. W. Toohey, W. H. Brune, R. J. Salawitch, A. E. Dessler, and J. G. Anderson (1993), Balloon-borne in situ measurements of ClO and ozone: Implications for heterogeneous chemistry and mid-latitude ozone loss, *Geophys. Res. Lett.*, **20**, 1795–1798.
- Baldwin, M. P., et al. (2001), The quasi-biennial oscillation, *Rev. Geophys.*, **39**, 179–229.
- Berthet, G., J. G. Esler, and P. H. Haynes (2007), A Lagrangian perspective of the tropopause and the ventilation of the lowermost stratosphere, *J. Geophys. Res.*, **112**, D18102, doi:10.1029/2006JD008295.
- Bloom, S. C., L. L. Takacs, A. M. da Silva, and D. Ledvina (1996), Data assimilation using incremental analysis updates, *Mon. Weather Rev.*, **124**, 1256–1271.
- Bönisch, H., A. Engel, J. Curtius, T. Birner, and P. Hoor (2009), Quantifying transport into the lowermost stratosphere using simultaneous in situ measurements of SF₆ and CO₂, *Atmos. Chem. Phys.*, **9**, 5905–5919.
- Borrmann, S., S. Solomon, J. E. Dye, and B. P. Luo (1996), The potential of cirrus clouds for heterogeneous chlorine activation, *Geophys. Res. Lett.*, **23**, 2133–2136.
- Borrmann, S., S. Solomon, L. Avallone, D. Toohey, and D. Baumgardner (1997), On the occurrence of ClO in cirrus clouds and volcanic aerosol in the tropopause region, *Geophys. Res. Lett.*, **24**, 2011–2014.
- Bosilovich, M. G., J. Chen, F. R. Robertson, and R. F. Adler (2008), Evaluation of global precipitation in reanalyses, *J. Appl. Meteorol. Climatol.*, **47**, 2279–2299.
- Bowman, K. P. (1993), Large-scale isentropic mixing properties of the Antarctic polar vortex from analyzed winds, *J. Geophys. Res.*, **98**, 23,013–23,027.
- Bowman, K. P., and A. J. Krueger (1985), A global climatology of total ozone from the Nimbus 7 Total Ozone Mapping Spectrometer, *J. Geophys. Res.*, **90**, 7967–7976.
- Brasseur, G. P., X. X. Tie, P. J. Rasch, and F. Lefèvre (1997), A three-dimensional simulation of the Antarctic ozone hole: Impact of anthropogenic chlorine on the lower stratosphere and upper troposphere, *J. Geophys. Res.*, **102**, 8909–8930.
- Bregman, A., et al. (1995), Aircraft measurements of O₃, HNO₃, and N₂O in the winter Arctic lower stratosphere during the Stratosphere-Troposphere Experiment by Aircraft Measurements (STREAM) 1, *J. Geophys. Res.*, **100**, 11,245–11,260.
- Bregman, A., M. van den Broek, K. S. Carslaw, R. Müller, T. Peter, M. P. Scheele, and J. Lelieveld (1997), Ozone depletion in the late winter lower Arctic stratosphere: Observations and model results, *J. Geophys. Res.*, **102**, 10,815–10,828.
- Bregman, A., J. Lelieveld, M. M. P. van den Broek, P. C. Siegmund, H. Fischer, and O. Bujok (2000), N₂O and O₃ relationship in the lowermost stratosphere: A diagnostic for mixing processes as represented by a three-dimensional chemistry-transport model, *J. Geophys. Res.*, **105**, 17,279–17,290.
- Bregman, A., M. C. Krol, H. Teyssèdre, W. A. Norton, A. Iwi, M. Chipperfield, G. Pitari, J. K. Sundet, and J. Lelieveld (2001), Chemistry-transport model comparison with ozone observations in the midlatitude lowermost stratosphere, *J. Geophys. Res.*, **106**, 17,479–17,496.
- Bregman, B., P.-H. Wang, and J. Lelieveld (2002), Chemical ozone loss in the tropopause region on subvisible ice clouds, calculated with a chemistry-transport model, *J. Geophys. Res.*, **107**(D3), 4032, doi:10.1029/2001JD000761.
- Brühl, C., P. J. Crutzen, and J.-U. Groß (1998), High-latitude, summertime NO_x activation and seasonal ozone decline in the lower stratosphere: Model calculations based on observations by HALOE on UARS, *J. Geophys. Res.*, **103**, 3587–3597.
- Brune, W. H., J. G. Anderson, and K. R. Chan (1989), In situ observations of ClO in the Antarctic: ER-2 aircraft results from 54°S to 72°S latitude, *J. Geophys. Res.*, **94**, 16,649–16,663.
- Brune, W. H., D. W. Toohey, J. G. Anderson, and K. R. Chan (1990), In situ observations of ClO in the Arctic stratosphere: ER-2 aircraft results from 59°N to 80°N latitude, *Geophys. Res. Lett.*, **17**, 505–508.
- Butchart, N., and E. E. Remsberg (1986), The area of the stratospheric polar vortex as a diagnostic for tracer transport on an isentropic surface, *J. Atmos. Sci.*, **43**, 1319–1339.
- Chen, P. (1994), The permeability of the Antarctic vortex edge, *J. Geophys. Res.*, **99**, 20,563–20,571.
- Chen, P. (1995), Isentropic cross-tropopause mass exchange in the extratropics, *J. Geophys. Res.*, **100**, 16,661–16,673.
- Chen, P., J. R. Holton, A. O'Neill, and R. Swinbank (1994), Quasi-horizontal transport and mixing in the Antarctic stratosphere, *J. Geophys. Res.*, **99**, 16,851–16,866.
- Chipperfield, M. P. (1999), Multiannual simulations with a three-dimensional chemical transport model, *J. Geophys. Res.*, **104**, 1781–1805.
- Chipperfield, M. P. (2003), A three-dimensional model study of long-term mid-high latitude lower stratosphere ozone changes, *Atmos. Chem. Phys.*, **3**, 1253–1265.
- Chipperfield, M. P., and L. J. Gray (1992), Two-dimensional model studies of the interannual variability of trace gases in the middle atmosphere, *J. Geophys. Res.*, **97**, 5963–5980.
- Collins, J. E., G. W. Sachse, B. E. Anderson, A. J. Weinheimer, J. G. Walega, and B. A. Ridley (1993), AASE-II in situ tracer correlations of methane, nitrous oxide, and ozone as observed aboard the DC-8, *Geophys. Res. Lett.*, **20**, 2543–2546.
- Dethof, A., A. O'Neill, and J. Slingo (2000), Quantification of the isentropic mass transport across the dynamical tropopause, *J. Geophys. Res.*, **105**, 12,279–12,293.
- de Zafra, R. L., J. M. Reeves, and D. T. Shindell (1995), Chlorine monoxide in the Antarctic spring vortex: 1. Evolution of midday vertical profiles over McMurdo Station, 1993, *J. Geophys. Res.*, **100**, 13,999–14,007.
- Dibb, J. E., E. Scheuer, M. Avery, J. Plant, and G. Sachse (2006), In situ evidence for renitrification in the Arctic lower stratosphere during the polar Aura validation experiment (PAVE), *Geophys. Res. Lett.*, **33**, L12815, doi:10.1029/2006GL026243.
- Douglass, A., and S. Kawa (1999), Contrast between 1992 and 1997 high-latitude spring Halogen Occultation Experiment observations of lower stratospheric HCl, *J. Geophys. Res.*, **104**(D15), 18,739–18,754.
- Douglass, A. R., R. B. Rood, J. A. Kaye, R. S. Stolarski, D. J. Allen, and E. M. Larson (1991), The influence of polar heterogeneous processes on reactive chlorine at middle latitudes: Three dimensional model implications, *Geophys. Res. Lett.*, **18**, 25–28.
- Douglass, A. R., M. R. Schoeberl, R. S. Stolarski, J. W. Waters, J. M. Russell, A. E. Roche, and S. T. Massie (1995), Interhemispheric differences in springtime production of HCl and ClONO₂ in the polar vortices, *J. Geophys. Res.*, **100**, 13,967–13,978.
- Eckman, R. S., W. L. Grose, R. E. Turner, and W. T. Blackshear (1996), Polar ozone depletion: A three-dimensional chemical modeling study of its long-term global impact, *J. Geophys. Res.*, **101**, 22,977–22,989.
- Fahey, D. W., and A. R. Ravishankara (1999), Summer in the stratosphere, *Science*, **285**, 208–210.
- Fahey, D. W., D. M. Murphy, K. K. Kelly, M. K. W. Ko, M. H. Proffitt, C. S. Eubank, G. V. Ferry, M. Loewenstein, and K. R. Chan (1989), Measurements of nitric oxide and total reactive nitrogen in the Antarctic stratosphere: Observations and chemical implications, *J. Geophys. Res.*, **94**, 16,665–16,681.
- Farman, J. C., R. J. Murgatroyd, A. M. Silnickas, and B. A. Thrush (1985), Ozone photochemistry in the Antarctic stratosphere in summer, *Q. J. R. Meteorol. Soc.*, **111**, 1013–1028.
- Fioletov, V. E., and T. G. Shepherd (2005), Summertime total ozone variations over middle and polar latitudes, *Geophys. Res. Lett.*, **32**, L04807, doi:10.1029/2004GL022080.
- Fischer, H., et al. (1997), Observations of high concentrations of total reactive nitrogen (NO_x) and nitric acid (HNO₃) in the lower Arctic stratosphere during the Stratosphere-Troposphere Experiment by Aircraft Measurements (STREAM) II campaign in February 1995, *J. Geophys. Res.*, **102**, 23,559–23,571.
- Folkins, I., P. Bernath, C. Boone, G. Lesins, N. Livesey, A. M. Thompson, K. Walker, and J. C. Witte (2006), Seasonal cycles of O₃, CO, and convective outflow at the tropical tropopause, *Geophys. Res. Lett.*, **33**, L16802, doi:10.1029/2006GL026602.
- Forster, P. M. F., and K. P. Shine (1997), Radiative forcing and temperature trends from stratospheric ozone changes, *J. Geophys. Res.*, **102**, 10,841–10,855.

- Froidevaux, L., J. W. Waters, W. G. Read, L. S. Elson, W. G. Read, D. A. Flower, and R. F. Jarnot (1994), Global ozone observations from UARS MLS: An overview of zonal mean results, *J. Atmos. Sci.*, **51**, 2846–2866.
- Froidevaux, L., et al. (2008a), Validation of Aura Microwave Limb Sounder stratospheric ozone measurements, *J. Geophys. Res.*, **113**, D15S20, doi:10.1029/2007JD008771.
- Froidevaux, L., et al. (2008b), Validation of Aura Microwave Limb Sounder HCl measurements, *J. Geophys. Res.*, **113**, D15S25, doi:10.1029/2007JD009025.
- Fromm, M., D. T. Lindsey, R. Servranckx, G. Yue, T. Trickl, R. Sica, P. Doucet, and S. Godin-Beekmann (2010), The untold story of pyrocumulonimbus, *Bull. Am. Meteorol. Soc.*, pp. 1193–1209, doi:10.1175/2010BAMS3004.1.
- Fromm, M. D., J. D. Lumpe, R. M. Bevilacqua, E. P. Shettle, J. Hornstein, S. T. Massie, and K. H. Fricke (1997), Observations of Antarctic polar stratospheric clouds by POAM II: 1994–1996, *J. Geophys. Res.*, **102**, 23,659–23,672.
- Fromm, M. D., R. M. Bevilacqua, J. Hornstein, E. P. Shettle, K. Hoppel, and J. D. Lumpe (1999), An analysis of Polar Ozone and Aerosol Measurement POAM II Arctic stratospheric cloud observations, 1993–1996, *J. Geophys. Res.*, **104**, 24,341–24,357.
- Fu, R., et al. (2006), Short circuit of water vapor and polluted air to the global stratosphere by convective transport over the Tibetan Plateau, *Proc. Natl. Acad. Sci. U.S.A.*, **103**, 5664–5669.
- Groß, J.-U., R. B. Pierce, P. J. Crutzen, W. L. Grose, and J. M. Russell (1997), Re-formation of chlorine reservoirs in Southern Hemisphere polar spring, *J. Geophys. Res.*, **102**, 13,141–13,152.
- Groß, J.-U., P. Konopka, and R. Müller (2005), Ozone chemistry during the 2002 Antarctic vortex split, *J. Atmos. Sci.*, **62**, 860–870.
- Haigh, J. D., and H. K. Roscoe (2009), The final warming date of the Antarctic polar vortex and influences on its interannual variability, *J. Clim.*, **22**, 5809–5819.
- Hanson, D., and K. Mauersberger (1988), Laboratory studies of the nitric acid trihydrate: Implications for the south polar stratosphere, *Geophys. Res. Lett.*, **15**, 855–858.
- Haynes, P., and E. Shuckburgh (2000a), Effective diffusivity as a diagnostic of atmospheric transport: 1. Stratosphere, *J. Geophys. Res.*, **105**, 22,777–22,794.
- Haynes, P., and E. Shuckburgh (2000b), Effective diffusivity as a diagnostic of atmospheric transport: 2. Troposphere and lower stratosphere, *J. Geophys. Res.*, **105**, 22,795–22,810.
- Hegglin, M. I., et al. (2006), Measurements of NO, NO_y, N₂O, and O₃ during SPURT: Implications for transport and chemistry in the lowermost stratosphere, *Atmos. Chem. Phys.*, **6**, 1331–1350.
- Hegglin, M. I., C. D. Boone, G. L. Manney, and K. A. Walker (2009), A global view of the extratropical tropopause transition layer from Atmospheric Chemistry Experiment Fourier Transform Spectrometer O₃, H₂O, and CO, *J. Geophys. Res.*, **114**, D00B11, doi:10.1029/2008JD009984.
- Hendricks, J., E. Lippert, H. Petry, and A. Ebel (1999), Heterogeneous reactions on and in sulfate aerosols: Implications for the chemistry of the midlatitude tropopause region, *J. Geophys. Res.*, **104**, 5531–5550.
- Highwood, E. J., B. J. Hoskins, and P. Berrisford (2000), Properties of the Arctic tropopause, *Q. J. R. Meteorol. Soc.*, **126**, 1515–1532.
- Hintsa, E. J., et al. (1998), Troposphere-to-stratosphere transport in the lowermost stratosphere from measurements of H₂O, CO₂, N₂O, and O₃, *Geophys. Res. Lett.*, **25**, 2655–2658.
- Hofmann, D. J., and T. Deshler (1991), Stratospheric cloud observations during formation of the Antarctic ozone hole in 1989, *J. Geophys. Res.*, **96**, 2897–2912.
- Holton, J. R., P. H. Haynes, M. E. McIntyre, A. R. Douglass, R. B. Rood, and L. Pfister (1995), Stratosphere-troposphere exchange, *Rev. Geophys.*, **33**, 403–439.
- Hoor, P., H. Fischer, and J. Lelieveld (2005), Tropical and extratropical tropospheric air in the lowermost stratosphere over Europe: A CO-based budget, *Geophys. Res. Lett.*, **32**, L07802, doi:10.1029/2004GL022018.
- Hübner, G., et al. (1990), Redistribution of reactive odd nitrogen in the lower Arctic stratosphere, *Geophys. Res. Lett.*, **17**, 453–456.
- Irie, H., M. Koike, Y. Kondo, G. E. Bodeker, M. Y. Danilin, and Y. Sasano (2001), Redistribution of nitric acid in the Arctic lower stratosphere during the winter of 1996–1997, *J. Geophys. Res.*, **106**, 23,139–23,150.
- Jimenez, C. J., H. C. Pumphrey, I. A. MacKenzie, G. L. Manney, M. L. Santee, M. J. Schwartz, R. S. Harwood, and J. W. Waters (2006), EOS MLS observations of dehydration in the 2004–2005 polar winters, *Geophys. Res. Lett.*, **33**, L16806, doi:10.1029/2006GL025926.
- Jin, J. J., et al. (2006), Denitrification in the Arctic winter 2004/2005: Observations from ACE-FTS, *Geophys. Res. Lett.*, **33**, L19814, doi:10.1029/2006GL027687.
- Keim, E. R., et al. (1996), Observations of large reductions in the NO/NO_y ratio near the mid-latitude tropopause and the role of heterogeneous chemistry, *Geophys. Res. Lett.*, **23**, 3223–3226.
- Kleinböhl, A., et al. (2005), Denitrification in the Arctic mid-winter 2004/2005 observed by airborne submillimeter radiometry, *Geophys. Res. Lett.*, **32**, L19811, doi:10.1029/2005GL023408.
- Knudsen, B. M., and J.-U. Groß (2000), Northern midlatitude stratospheric ozone dilution in spring modeled with simulated mixing, *J. Geophys. Res.*, **105**, 6885–6890.
- Knudsen, B. M., et al. (1998), Ozone depletion in and below the Arctic vortex for 1997, *Geophys. Res. Lett.*, **25**, 627–630.
- Koike, M., et al. (2002), Redistribution of reactive nitrogen in the Arctic lower stratosphere in the 1999/2000 winter, *J. Geophys. Res.*, **107**(D20), 8275, doi:10.1029/2001JD001089.
- Kondo, Y., T. Sugita, M. Koike, S. R. Kawa, M. Y. Danilin, J. M. Rodriguez, S. Spreng, K. Golinger, and F. Arnold (2000), Partitioning of reactive nitrogen in the midlatitude lower stratosphere, *J. Geophys. Res.*, **105**, 1417–1424.
- Konopka, P., J.-U. Groß, S. Bausch, R. Müller, D. S. McKenna, O. Morgenstern, and Y. Orsolini (2003), Dynamics and chemistry of vortex remnants in late Arctic spring 1997 and 2000: Simulations with the Chemical Lagrangian Model of the Stratosphere (CLaMS), *Atmos. Chem. Phys.*, **3**, 839–849.
- Konopka, P., J.-U. Groß, G. Günther, F. Ploeger, R. Pommrich, R. Müller, and N. Livesey (2010), Annual cycle of ozone at and above the tropical tropopause: observations versus simulations with the Chemical Lagrangian Model of the Stratosphere (CLaMS), *Atmos. Chem. Phys.*, **10**, 121–132.
- Krebsbach, M., C. Schiller, D. Brunner, G. Günther, M. I. Hegglin, D. Mottaghy, M. Riese, N. Spelten, and H. Wernli (2006), Seasonal cycles and variability of O₃ and H₂O in the UT/LMS during SPURT, *Atmos. Chem. Phys.*, **6**, 109–125.
- Kunz, A., P. Konopka, R. Müller, and L. L. Pan (2011), The dynamical tropopause based on isentropic potential vorticity gradients, *J. Geophys. Res.*, **116**, D01110, doi:10.1029/2010JD014343.
- Lacis, A. A., D. J. Wuebbles, and J. A. Logan (1990), Radiative forcing of climate by changes in the vertical distribution of ozone, *J. Geophys. Res.*, **95**, 9971–9981.
- Lee, A. M., R. L. Jones, I. Kilbane-Dawe, and J. A. Pyle (2002), Diagnosing ozone loss in the extratropical lower stratosphere, *J. Geophys. Res.*, **107**(D11), 4110, doi:10.1029/2001JD000538.
- Lee, J. N., D. L. Wu, G. L. Manney, M. J. Schwartz, A. Lambert, N. J. Livesey, K. R. Minschwaner, H. C. Pumphrey, and W. G. Read (2011), Aura Microwave Limb Sounder observations of the polar middle atmosphere: Dynamics and transport of CO and H₂O, *J. Geophys. Res.*, **116**, D05110, doi:10.1029/2010JD014608.
- Lelieveld, J., A. Bregman, F. Arnold, V. Bürger, P. J. Crutzen, H. Fischer, A. Waibel, P. Siegmund, and P. F. J. van Velthoven (1997), Chemical perturbation of the lowermost stratosphere through exchange with the troposphere, *Geophys. Res. Lett.*, **24**, 603–606.
- Lelieveld, J., A. Bregman, H. A. Scheeren, J. Ström, K. S. Carslaw, H. Fischer, P. Siegmund, and F. Arnold (1999), Chlorine activation and ozone destruction in the northern lowermost stratosphere, *J. Geophys. Res.*, **104**, 8201–8213.
- Livesey, N. J., W. V. Snyder, W. G. Read, and P. A. Wagner (2006), Retrieval algorithms for the EOS Microwave Limb Sounder (MLS), *IEEE Trans. Geosci. Remote Sens.*, **44**, 1144–1155.
- Livesey, N. J., et al. (2008a), Validation of Aura Microwave Limb Sounder O₃ and CO observations in the upper troposphere and lower stratosphere, *J. Geophys. Res.*, **112**, D15S02, doi:10.1029/2007JD008805.
- Livesey, N. J., et al. (2008b), Version 2.2 Level 2 data quality and description document, *Tech. Rep. JPL D-32381*, Jet Propul. Lab., Pasadena, Calif. (Available from <http://mls.jpl.nasa.gov/>.)
- Livesey, N. J., et al. (2011), Version 3.3 Level 2 data quality and description document, *Tech. Rep. JPL D-33509*, Jet Propul. Lab., Pasadena, Calif. (Available from <http://mls.jpl.nasa.gov/>.)
- Logan, J. A. (1999), An analysis of ozonesonde data for the lower stratosphere: Recommendations for testing models, *J. Geophys. Res.*, **104**, 16,151–16,170.
- Manney, G. L., R. W. Zurek, A. O'Neill, and R. Swinbank (1994), On the motion of air through the stratospheric polar vortex, *J. Atmos. Sci.*, **51**, 2973–2994.
- Manney, G. L., H. A. Michelsen, M. L. Santee, M. R. Gunson, F. W. Irion, A. E. Roche, and N. J. Livesey (1999), Polar vortex dynamics during spring and fall diagnosed using trace gas observations from the Atmospheric Trace Molecule Spectroscopy instrument, *J. Geophys. Res.*, **104**, 18,841–18,866.
- Manney, G. L., M. L. Santee, N. J. Livesey, L. Froidevaux, H. C. Pumphrey, W. G. Read, and J. W. Waters (2005), EOS Microwave

- Limb Sounder observations of the Antarctic polar vortex breakup in 2004, *Geophys. Res. Lett.*, 32, L12811, doi:10.1029/2005GL022823.
- Manney, G. L., et al. (2007), Solar occultation satellite data and derived meteorological products: Sampling issues and comparisons with Aura Microwave Limb Sounder, *J. Geophys. Res.*, 112, D24S50, doi:10.1029/2007JD008709.
- Manney, G. L., M. J. Schwartz, K. Krüger, M. L. Santee, S. Pawson, J. N. Lee, W. H. Daffer, R. A. Fuller, and N. J. Livesey (2009a), Aura Microwave Limb Sounder observations of dynamics and transport during the record-breaking 2009 Arctic stratospheric major warming, *Geophys. Res. Lett.*, 36, L12815, doi:10.1029/2009GL038586.
- Manney, G. L., et al. (2009b), Satellite observations and modeling of transport in the upper troposphere through the lower mesosphere during the 2006 major stratospheric sudden warming, *Atmos. Chem. Phys.*, 9, 4775–4795.
- Manney, G. L., et al. (2011), Jet characterization in the upper troposphere/lower stratosphere (UTLS): Applications to climatology and transport studies, *Atmos. Chem. Phys.*, 11, 6115–6137.
- Marchand, M., S. Godin, A. Hauchecorne, F. Lefèvre, S. Bekki, and M. Chipperfield (2003), Influence of polar ozone loss on northern mid-latitude regions estimated by a high-resolution chemistry transport model during winter 1999/2000, *J. Geophys. Res.*, 108(D5), 8326, doi:10.1029/2001JD000906.
- Marcy, T. P., et al. (2004), Quantifying stratospheric ozone in the upper troposphere with in situ measurements of HCl, *Science*, 304, 261–265.
- Marcy, T. P., et al. (2007), Measurements of trace gases in the tropical tropopause layer, *Atmos. Environ.*, 41, 7253–7261.
- Massoli, P., M. Maturilli, and R. Neuber (2006), Climatology of Arctic polar stratospheric clouds as measured by lidar in Ny-Ålesund, Spitsbergen (79°N, 12°E), *J. Geophys. Res.*, 111, D09206, doi:10.1029/2005JD005840.
- McDonald, M., R. L. de Zafra, and G. Muscari (2000), Millimeter wave spectroscopic measurements over the South Pole: 5. Morphology and evolution of HNO₃ vertical distribution, 1993 versus 1995, *J. Geophys. Res.*, 105, 17,739–17,750.
- McElroy, M. B., and R. J. Salawitch (1989), Changing composition of the global stratosphere, *Science*, 243, 763–770.
- McIntyre, M. E. (1995), The stratospheric polar vortex and sub-vortex: fluid dynamics and midlatitude ozone loss, *Philos. Trans. R. Soc. London, A*, 352, 227–240.
- Mickley, L. J., J. P. D. Abbatt, J. E. Frederick, and J. M. Russell (1997), Evolution of chlorine and nitrogen species in the lower stratosphere during Antarctic spring: Use of tracers to determine chemical change, *J. Geophys. Res.*, 102, 21,479–21,491.
- Millard, G. A., A. M. Lee, and J. A. Pyle (2003), A model study of the connection between polar and midlatitude ozone loss in the Northern Hemisphere lower stratosphere, *J. Geophys. Res.*, 107(D5), 8323, doi:10.1029/2001JD000899.
- Murphy, D. M. (1991), Ozone loss rates calculated along ER-2 flight tracks, *J. Geophys. Res.*, 96, 5045–5053.
- Murphy, D. M., D. W. Fahey, M. H. Proffitt, S. C. Liu, K. R. Chan, C. S. Eubank, S. R. Kawa, and K. K. Kelly (1993), Reactive nitrogen and its correlation with ozone in the lower stratosphere and upper troposphere, *J. Geophys. Res.*, 98, 8751–8773.
- Nakamura, N. (1996), Two-dimensional mixing, edge formation, and permeability diagnosed in area coordinates, *J. Atmos. Sci.*, 53, 1524–1537.
- Norton, W. A., and M. P. Chipperfield (1995), Quantification of the transport of chemically activated air from the northern hemisphere polar vortex, *J. Geophys. Res.*, 100, 25,817–25,840.
- Pan, L. L., S. Solomon, W. Randel, J.-F. Lamarque, P. Hess, J. Gille, E.-W. Chiou, and M. P. McCormick (1997), Hemispheric asymmetries and seasonal variations of the lowermost stratospheric water vapor and ozone derived from SAGE II data, *J. Geophys. Res.*, 102, 28,177–28,184.
- Pan, L. L., W. J. Randel, B. L. Gary, M. J. Mahoney, and E. J. Hintsa (2004), Definitions and sharpness of the extratropical tropopause: A trace gas perspective, *J. Geophys. Res.*, 109, D23103, doi:10.1029/2004JD004982.
- Pan, L. L., J. C. Wei, D. E. Kinnison, R. R. Garcia, D. J. Wuebbles, and G. P. Brasseur (2007), A set of diagnostics for evaluating chemistry-climate models in the extratropical tropopause region, *J. Geophys. Res.*, 112, D09316, doi:10.1029/2006JD007792.
- Park, J. H., and J. M. Russell (1994), Summer polar chemistry observations in the stratosphere made by HALOE, *J. Atmos. Sci.*, 51, 2903–2913.
- Perliski, L. M., S. Solomon, and J. London (1989), On the interpretation of seasonal variations of stratospheric ozone, *Planet. Space Sci.*, 37, 1527–1538.
- Piani, C., W. A. Norton, A. M. Iwi, E. A. Ray, and J. W. Elkins (2002), Transport of ozone-depleted air on the breakup of the stratospheric polar vortex in spring/summer 2000, *J. Geophys. Res.*, 107(D20), 8270, doi:10.1029/2001JD000488.
- Pittman, J. V., et al. (2007), Transport in the subtropical lowermost stratosphere during the Cirrus Regional Study of Tropical Anvils and Cirrus Layers—Florida Area Cirrus Experiment, *J. Geophys. Res.*, 112, D08304, doi:10.1029/2006JD007851.
- Pitts, M. C., L. R. Poole, and L. W. Thomason (2009), CALIPSO polar stratospheric cloud observations: second-generation detection algorithm and composition discrimination, *Atmos. Chem. Phys.*, 9, 7577–7589.
- Popp, P., et al. (2009), Stratospheric correlation between nitric acid and ozone, *J. Geophys. Res.*, 114, D03305, doi:10.1029/2008JD010875.
- Poulida, O., R. R. Dickerson, and A. Heymsfield (1996), Stratosphere-troposphere exchange in a midlatitude mesoscale convective complex: 1. Observations, *J. Geophys. Res.*, 101, 6823–6836.
- Prados, A. I., G. E. Nedoluha, R. M. Bevilacqua, D. R. Allen, K. W. Hoppe, and A. Marenco (2003), POAM III ozone in the upper troposphere and lowermost stratosphere: Seasonal variability and comparisons to aircraft observations, *J. Geophys. Res.*, 108(D7), 4218, doi:10.1029/2002JD002819.
- Prather, M., and A. H. Jaffe (1990), Global impact of the Antarctic ozone hole: Chemical propagation, *J. Geophys. Res.*, 95, 3473–3492.
- Proffitt, M. H., A. Aikin, J. J. Margitan, M. Loewenstein, J. R. Podolske, A. Weaver, K. R. Chan, H. Fast, and J. W. Elkins (1993), Ozone loss inside the northern polar vortex during the 1991–1992 winter, *Science*, 261, 1150–1154.
- Randel, W. J., M. Park, F. Wu, and N. Livesey (2007), A large annual cycle in ozone above the tropical tropopause linked to the Brewer-Dobson circulation, *J. Atmos. Sci.*, 64, 4479–4488.
- Ray, E. A., F. L. Moore, J. W. Elkins, G. S. Dutton, D. W. Fahey, H. Vömel, S. J. Oltmans, and K. H. Rosenlof (1999), Transport into the Northern Hemisphere lowermost stratosphere revealed by in situ tracer measurements, *J. Geophys. Res.*, 104, 26,565–26,580.
- Reinecker, M. M., et al. (2008), The GEOS-5 data assimilation system—Documentation of versions 5.0.1 and 5.1.0, *NASA Tech. Memo.*, TM-2007-104606, vol. 27.
- Reinecker, M. M., et al. (2011), MERRA—NASA's Modern-Era Retrospective Analysis for Research and Applications, *J. Clim.*, 24, 3624–3648, doi:10.1175/JCLI-D-11-00015.1.
- Rex, M., et al. (2006), Arctic winter 2005: Implications for stratospheric ozone loss and climate change, *Geophys. Res. Lett.*, 33, L23808, doi:10.1029/2006GL026731.
- Rogal, M., M. H. Hitchman, M. L. Baker, G. J. Tripoli, I. Stajner, and H. Hayashi (2010), Modeling the effects of Southeast Asian monsoon outflow on subtropical anticyclones and midlatitude ozone over the Southern Indian Ocean, *J. Geophys. Res.*, 115, D20101, doi:10.1029/2009JD012979.
- Rood, R. B., A. R. Douglass, M. C. Cerniglia, and W. G. Read (1997), Synoptic-scale mass exchange from the troposphere to the stratosphere, *J. Geophys. Res.*, 102, 23,467–23,485.
- Rosenlof, K. H. (1995), Seasonal cycle of the residual mean meridional circulation in the stratosphere, *J. Geophys. Res.*, 100, 5173–5191.
- Rosenlof, K. H., A. F. Tuck, K. K. Kelly, J. M. Russell, and M. P. McCormick (1997), Hemispheric asymmetries in water vapor and inferences about transport in the lower stratosphere, *J. Geophys. Res.*, 102, 13,213–13,234.
- Santee, M. L., G. L. Manney, L. Froidevaux, W. G. Read, and J. W. Waters (1999), Six years of UARS Microwave Limb Sounder HNO₃ observations: Seasonal, interhemispheric, and interannual variations in the lower stratosphere, *J. Geophys. Res.*, 104, 8225–8246.
- Santee, M. L., G. L. Manney, J. W. Waters, and N. J. Livesey (2003), Variations and climatology of ClO in the polar lower stratosphere from UARS Microwave Limb Sounder measurements, *J. Geophys. Res.*, 108(D15), 4454, doi:10.1029/2002JD003335.
- Santee, M. L., et al. (2007), Validation of the Aura Microwave Limb Sounder HNO₃ measurements, *J. Geophys. Res.*, 112, D24S40, doi:10.1029/2007JD008721.
- Santee, M. L., et al. (2008a), Validation of the Aura Microwave Limb Sounder ClO measurements, *J. Geophys. Res.*, 113, D15S22, doi:10.1029/2007JD008762.
- Santee, M. L., et al. (2008b), A study of stratospheric chlorine partitioning based on new satellite measurements and modeling, *J. Geophys. Res.*, 113, D12307, doi:10.1029/2007JD009057.
- Sassi, F., D. Kinnison, B. A. Boville, R. R. Garcia, and R. Roble (2004), Effect of El Niño–Southern Oscillation on the dynamical, thermal, and chemical structure of the middle atmosphere, *J. Geophys. Res.*, 109, D17108, doi:10.1029/2003JD004434.
- Schoeberl, M. R. (2004), Extratropical stratosphere-troposphere mass exchange, *J. Geophys. Res.*, 109, D13303, doi:10.1029/2004JD004525.

- Schoeberl, M. R., et al. (2006), Chemical observations of a polar vortex intrusion, *J. Geophys. Res.*, **111**, D20306, doi:10.1029/2006JD007134.
- Scott, R. K., E. F. Shuckburgh, J.-P. Cammas, and B. Legras (2003), Stretching rates and equivalent length near the tropopause, *J. Geophys. Res.*, **108**(D13), 4394, doi:10.1029/2002JD002988.
- Seo, K.-H., and K. P. Bowman (2001), A climatology of isentropic cross-tropopause exchange, *J. Geophys. Res.*, **106**, 28,159–28,172.
- Shepherd, T. G. (2007), Transport in the middle atmosphere, *J. Meteorol. Soc. Jpn. B*, **85**, 165–191.
- Shuckburgh, E., F. d'Ovidio, and B. Legras (2009), Local mixing events in the upper troposphere and lower stratosphere. Part II: Seasonal and interannual variability, *J. Atmos. Sci.*, **66**, 3695–3706.
- Solomon, P., J. Barrett, B. Connor, S. Zoonematkermani, A. Parrish, A. Lee, J. Pyle, and M. Chipperfield (2000), Seasonal observations of chlorine monoxide in the stratosphere over Antarctica during the 1996–1998 ozone holes and comparison with the SLIMCAT three-dimensional model, *J. Geophys. Res.*, **105**, 28,979–29,001.
- Solomon, P., B. Connor, J. Barrett, T. Mooney, A. Lee, and A. Parrish (2002), Measurements of stratospheric ClO over Antarctica in 1996–2000 and implications for ClO dimer chemistry, *Geophys. Res. Lett.*, **29**(15), 1708, doi:10.1029/2002GL015232.
- Solomon, S., S. Borrman, R. R. Garcia, R. W. Portmann, L. W. Thomason, L. R. Poole, D. Winker, and M. P. McCormick (1997), Heterogeneous chlorine chemistry in the tropopause region, *J. Geophys. Res.*, **102**, 21,411–21,429.
- Spackman, J. R., E. M. Weinstock, J. G. Anderson, D. F. Hurst, H.-J. Jost, and S. M. Schaufler (2007), Aircraft observations of rapid meridional transport from the tropical tropopause layer into the lowermost stratosphere: Implications for midlatitude ozone, *J. Geophys. Res.*, **112**, D12308, doi:10.1029/2006JD007618.
- Stohl, A., et al. (2003), Stratosphere-troposphere exchange: A review, and what we have learned from STACCATO, *J. Geophys. Res.*, **108**(D12), 8516, doi:10.1029/2002JD002490.
- Sze, N. D., M. K. W. Ko, D. K. Weisenstein, J. M. Rodriguez, R. S. Stolarski, and M. R. Schoeberl (1989), Antarctic ozone hole: Possible implications for ozone trends in the Southern Hemisphere, *J. Geophys. Res.*, **94**, 11,521–11,528.
- Tabazadeh, A., M. L. Santee, M. Y. Danilin, H. C. Pumphrey, P. A. Newman, P. J. Hamill, and J. L. Mergenthaler (2000), Quantifying denitrification and its effect on ozone recovery, *Science*, **288**, 1407–1411.
- Thornton, B. F., D. W. Toohey, L. M. Avallone, H. Harder, M. Martinez, J. B. Simpass, W. H. Brune, and M. A. Avery (2003), In situ observations of ClO near the winter polar tropopause, *J. Geophys. Res.*, **108**(D8), 8333, doi:10.1029/2002JD002839.
- Thornton, B. F., et al. (2007), Chlorine activation near the midlatitude tropopause, *J. Geophys. Res.*, **112**, D18306, doi:10.1029/2006JD007640.
- Tilmes, S., R. Müller, R. J. Salawitch, U. Schmidt, C. R. Webster, H. Oelhaf, C. C. Camy-Peyret, and J. M. Russell (2008), Chemical ozone loss in the Arctic winter 1991–1992, *Atmos. Chem. Phys.*, **8**, 1897–1910.
- Trenberth, K. E. (1997), The definition of El Niño, *Bull. Am. Meteorol. Soc.*, **78**, 2771–2777.
- Tuck, A. F. (1989), Synoptic and chemical evolution of the Antarctic vortex in late winter and early spring, 1987, *J. Geophys. Res.*, **94**, 11,687–11,737.
- Wang, P.-H., D. M. Cunnold, J. M. Zawodny, R. B. Pierce, J. R. Olson, G. S. Kent, and K. M. Skeens (1998), Seasonal variations in the isentropic layer between 330 and 380 K as observed by SAGE II: Implications of extratropical cross-tropopause transport, *J. Geophys. Res.*, **103**, 28,647–28,659.
- Wang, P.-H., D. M. Cunnold, C. R. Trepte, H. J. Wang, P. Jing, J. Fishman, V. G. Brackett, J. M. Zawodney, and G. E. Bodeker (2006), Ozone variability in the midlatitude upper troposphere and lower stratosphere diagnosed from a monthly SAGE II climatology relative to the tropopause, *J. Geophys. Res.*, **111**, D21304, doi:10.1029/2005JD006108.
- Waters, J. W., L. Froidevaux, W. G. Read, G. L. Manney, L. S. Elson, D. A. Flower, R. F. Jarnot, and R. S. Harwood (1993), Stratospheric ClO and ozone from the Microwave Limb Sounder on the Upper Atmosphere Research Satellite, *Nature*, **362**, 597–602.
- Waters, J. W., et al. (2006), The Earth Observing System Microwave Limb Sounder (EOS MLS) on the Aura satellite, *IEEE Trans. Geosci. Remote Sens.*, **44**, 1075–1092.
- Waugh, D. W., et al. (1997), Mixing of polar vortex air into middle latitudes as revealed by tracer-tracer scatterplots, *J. Geophys. Res.*, **102**, 13,119–13,134.
- World Meteorological Organization (2007a), Scientific assessment of ozone depletion: 2006, *Rep. 50*, Global Ozone Res. and Monit. Proj., Geneva, Switzerland.
- World Meteorological Organization (2007b), Antarctic ozone bulletin, 2006 winter/spring summary, *Tech. Rep. 8*, Global Atmos. Watch Programme, Geneva, Switzerland. (Available at <http://www.wmo.int/pages/prog/arep/gaw/ozone/index.html>)
- World Meteorological Organization (2008), Antarctic ozone bulletin, 2008, *Tech. Rep. 3*, Global Atmos. Watch Programme, Geneva, Switzerland. (Available at <http://www.wmo.int/pages/prog/arep/gaw/ozone/index.html>)
- Wu, W.-S., R. J. Purser, and D. F. Parrish (2002), Three-dimensional variational analysis with spatially inhomogeneous covariances, *Mon. Weather Rev.*, **130**, 2905–2916.
- Yang, E.-S., D. M. Cunnold, R. J. Salawitch, M. P. McCormick, R. Russell, J. M. Zawodny, S. Oltmans, and M. J. Newchurch (2006), Attribution of recovery in lower-stratospheric ozone, *J. Geophys. Res.*, **111**, D17309, doi:10.1029/2005JD006371.
- Zhou, S., M. E. Gelman, A. J. Miller, and J. P. McCormack (2000), An interhemispheric comparison of the persistent stratospheric polar vortex, *Geophys. Res. Lett.*, **27**, 1123–1126.

L. Froidevaux, N. J. Livesey, W. G. Read, M. L. Santee, and M. J. Schwartz, Jet Propulsion Laboratory, Mail Stop 183-701, 4800 Oak Grove Drive, Pasadena, CA 91109, USA. (Michelle.L.Santee@jpl.nasa.gov)

G. L. Manney, Department of Physics, New Mexico Institute of Mining and Technology, Workman Center, 801 Leroy Pl., Socorro, NM 87801, USA.